

AD-761 999

BUBBLE TRANSPORT THEORY WITH APPLICATION
TO THE UPPER OCEAN

Garrett A. Garrettson

Naval Postgraduate School
Monterey, California

6 April 1973

DISTRIBUTED BY:

NTIS

National Technical Information Service
U. S. DEPARTMENT OF COMMERCE
5285 Port Royal Road, Springfield Va. 22151

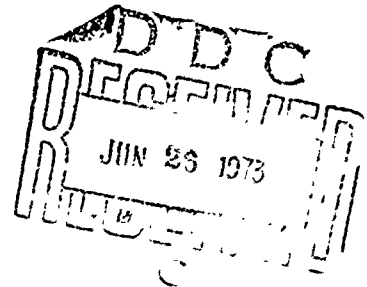
DISCLAIMER NOTICE

**THIS DOCUMENT IS BEST QUALITY
PRACTICABLE. THE COPY FURNISHED
TO DTIC CONTAINED A SIGNIFICANT
NUMBER OF PAGES WHICH DO NOT
REPRODUCE LEGIBLY.**

NAVAL POSTGRADUATE SCHOOL

Monterey, California

AD 761999



6 April 1973

NPS-61Gr73041A

Bubble Transport Theory With Application
to the Upper Ocean

G.A. Garrettson

Physics & Chemistry
Department

Approved for public release; distribution unlimited.

Reproduced by
NATIONAL TECHNICAL
INFORMATION SERVICE
U.S. Department of Commerce
Springfield VA 22151

Unclassified

Security Classification

DOCUMENT CONTROL DATA - R & D

(Security classification of title, body of abstract and indexes annotation must be entered when the overall report is classified)

1. ORIGINATING ACTIVITY (Corporate author)

Naval Postgraduate School
Monterey, California 93940

2a. REPORT SECURITY CLASSIFICATION

Unclassified

2b. GROUP

3. REPORT TITLE

Bubble Transport Theory with Application to the Upper Ocean

4. DESCRIPTIVE NOTES (Type of report and, inclusive dates)

Technical Report, NPS61Gr73041A, 6 April 1973

5. AUTHOR(S) (First name, middle initial, last name)

Garrett A. Garrettson

6. REPORT DATE

April 1973

7a. TOTAL NO OF PAGES

66 62

7b. NO OF REFS

20

8a. CONTRACT OR GRANT NO.

b. PROJECT NO

c.

d.

9a. ORIGINATOR'S REPORT NUMBER(S)

9b. OTHER REPORT NO(S) (Any other numbers that may be assigned this report)

10. DISTRIBUTION STATEMENT

Approved for public release; distribution unlimited.

11. SUPPLEMENTARY NOTES

12. SPONSORING MILITARY ACTIVITY

Naval Postgraduate School
Monterey, California 93940

13. ABSTRACT

The formalism of transport theory is adapted to a general description of bubble populations in a moving fluid. The bubble distribution, as a function of position, velocity, radius, and time, satisfies a Boltzmann-type transport equation that is derived and then formally solved by the method of characteristics. Before this new analytical tool can be applied, properties of the medium must be specified and a bubble dynamics model must be chosen. General expressions are written for bubble acceleration and radius change rate, and known models of bubble gas diffusion and drag are summarized for gas bubbles in liquids. Application to the upper ocean is discussed and then illustrated with some sample calculations. Explicit solutions are written for a steady-state, one dimensional ocean with distributed sources; the results clarify relations between observed bubble populations, proposed bubble source mechanisms, and known models of single bubble dynamics. This research was supported by: Naval Ship Systems Command, Code (PMS 302).

DD FORM 1473

1 NOV 65

(PAGE 1)

5/N 0101-807-6811

65

Unclassified

Security Classification

A-31408

1a

14. KEY WORDS	LINK A		LINK B		LINK C	
	ROLE	WT	ROLE	WT	ROLE	WT
Bubble Dynamics						
Transport Theory						
Ocean Bubbles						

NAVAL POSTGRADUATE SCHOOL
Monterey, California

Rear Admiral M. B. Freeman
Superintendent

M. U. Clauser
Provost

TITLE: Bubble Transport Theory with Application to the Upper Ocean *

AUTHOR: Garrett A. Garrettson

ABSTRACT:

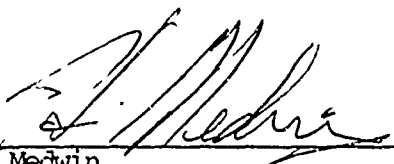
The formalism of transport theory is adapted to a general description of bubble populations in a moving fluid. The bubble distribution, as a function of position, velocity, radius, and time, satisfies a Boltzmann-type transport equation that is derived and then formally solved by the method of characteristics. Before this new analytical tool can be applied, properties of the medium must be specified and a bubble dynamics model must be chosen. General expressions are written for bubble acceleration and radius change rate, and known models of bubble gas diffusion and drag are summarized for gas bubbles in liquids. Application to the upper ocean is discussed and then illustrated with some sample calculations. Explicit solutions are written for a steady-state, one dimensional ocean with distributed sources; the results clarify relations between observed bubble populations, proposed bubble source mechanisms, and known models of single bubble dynamics.

This research was supported by: Naval Ship Systems Command, Code (PMS 302).

Approved by:

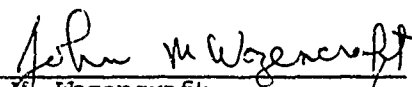


O. Heinz
Chairman
Department of Physics and Chemistry



H. Medwin
Professor of Physics
Principal Investigator

Released by:



J. M. Wozencraft
Dean of Research

*An abridged version of this report will appear in the Journal of Fluid Mechanics.

NPS-61Gr73041A
6 April 1973

TABLE OF CONTENTS

I.	INTRODUCTION-----	5
II.	THE BUBBLE TRANSPORT EQUATION-----	7
III.	SOLUTION BY METHOD OF CHARACTERISTICS-----	13
	A. LAGRANGIAN AND EULERIAN REPRESENTATIONS-----	14
	B. FORMAL SOLUTION-----	15
IV.	SINGLE BUBBLE DYNAMICS-----	19
	A. ACCELERATION-----	19
	B. DRAG ON GAS BUBBLES IN A LIQUID-----	20
	C. RADIUS CHANGE RATE-----	21
	D. GAS DIFFUSION-----	22
V.	APPLICATION TO THE UPPER OCEAN-----	25
	A. BUBBLE SOURCES AND FLUID VELOCITY FIELDS-----	25
	B. EXAMPLE-----	27
	1. Characteristic Curves-----	29
	2. Bubble Distributions-----	34
	3. Numerical Results-----	38
VI.	CONCLUSION-----	42
	APPENDIX-----	43
	REFERENCES-----	46
	FIGURE CAPTIONS-----	47
	FIGURES-----	49
	INITIAL DISTRIBUTION LIST-----	61
	FORM DD 1473-----	65

ACKNOWLEDGEMENTS

The author would like to thank several people who aided this research effort: Professor Herman Medwin supplied valuable suggestions and information concerning bubble phenomena in the upper ocean; LT. Frank H. Heistand, USN, aided in the preliminary investigations of single bubble dynamics and provided programming support; LT. Thomas C. Vajda, USN, supplied programming support for obtaining the numerical results of Section V; Mrs. Clarey and Mrs. Sutherland (NPS) diligently typed the manuscript; and my wife Gloria typed corrections and gave the necessary moral support.

This research was partially supported by the Naval Ship Systems Command, Code (PMS 302).

I. INTRODUCTION

The solutions of many experimental and engineering problems depend upon a knowledge of bubble distributions in a fluid medium. For instance, gas bubbles near the surface of the ocean are important in a variety of subjects that include underwater sound propagation (Shulkin 1968 & 1969), meteorology (Blanchard & Woodcock 1957), sea surface chemistry (Sutcliffe, et al 1963), cavitation (Fox and Herzfeld 1954), and air-sea gas exchange (Karwisher 1963). Several efforts have been made to measure bubble densities in the ocean (Blanchard & Woodcock 1957; Glotov, et al 1962; McCartney and Bary 1965), the most recent made by Medwin (1970). To infer near surface bubble populations from in-situ measurements of acoustic attenuation, Medwin exploited the fact that a gas bubble's scattering and absorption cross sections for sound at the bubble resonant frequency can typically be 1000 times its geometrical cross section. For this reason large bubble densities near the sea surface can significantly affect underwater sound transmission.

Many complex factors affect bubble distributions in a fluid such as the ocean, and some of these phenomena have been carefully investigated. For example, LeBlond (1969) examined gas diffusion from an ascending bubble, and Levich (1962, Ch. 8) is an excellent reference on single bubble dynamics. The purpose of this paper is to develop and to demonstrate new analytical tools for investigating relationships between observed bubble distributions and the phenomena which create, transport, and eliminate bubbles.

In sections two and three the formalism of transport theory is adapted to the general problem of describing bubble populations in a moving fluid. The bubble distribution, as a function of position, time, velocity, and radius, satisfies a Boltzmann-type transport equation that is derived. Using a Lagrangian viewpoint, the formal solution is expressed as a line integral of the volume source function along characteristic curves. In section four general

expressions are obtained for bubble acceleration and radius change rate and some known models of gas diffusion and bubble drag are introduced. Finally, in the context of gas bubble transport in the upper ocean, a simple model is chosen to illustrate the utility of transport theory. Calculated results clarify relationships between observed bubble distributions, proposed bubble source mechanisms, and known models of single bubble dynamics.

II. THE BUBBLE TRANSPORT EQUATION

Consider the problem of describing the bubble distribution — as a function of position, \vec{r} , velocity, \vec{v} , size, ℓ , and time, t — in a moving fluid that may contain bubble sources and sinks. In general, a "bubble" might be considered any simple, closed region containing a fluid somehow different from that of the transporting medium. Since examples chosen in this paper refer primarily to spherical gas bubbles, ℓ will represent the bubble radius. However, if the bubbles are not spherical, then ℓ might represent the radius of a spherical volume equal to the actual bubble volume, or one might wish to generalize the description to include more than one parameter for size.

Suppose that the time evolution of the position, the velocity, and the radius of each bubble depends only upon the properties of the medium and the bubble characteristics and is statistically independent of the state of any other bubble. Then define the bubble distribution function, $\psi(\vec{r}, \vec{v}, \ell, t) d^3r d^3v d\ell$, as the mean number of bubbles at time t in the volume d^3r about \vec{r} , with velocity in d^3v about \vec{v} and the radius in $d\ell$ about ℓ .^{*} Furthermore, if bubbles interact with one another, suppose that no more than two interact at any one time and that the collision time is short compared to the time for ψ to change appreciably. Then ψ satisfies a Boltzmann-type transport equation whose solution describes the ensemble average behavior of the bubble population in terms of single bubble behavior.

At this point it is convenient to define the seven-dimensional volume element $d^7\tau \equiv d^3r d^3v d\ell$ and to adopt a Lagrangian viewpoint. In the time interval $(t, t+dt)$ the bubbles that were in $d^7\tau$ about (\vec{r}, \vec{v}, ℓ) have moved to a new volume

^{*}E.g., in the Cartesian representation, position components lie in the intervals $(x, x+dx)$, $(y, y+dy)$, and $(z, z+dz)$; velocity components lie in the intervals (v_x, v_x+dv_x) , (v_y, v_y+dv_y) , and (v_z, v_z+dv_z) ; and the radius is in the interval $(\ell, \ell+d\ell)$.

$d^7\tau$ about $(\vec{r}', \vec{v}', \ell')$, where the primed quantities refer to the time $t+dt$ and the unprimed quantities refer to the time t . This transport occurs by a change in position due to a velocity, $\vec{v} \equiv d\vec{r}/dt$, by a change in velocity due to an acceleration, $\vec{a} \equiv d\vec{v}/dt$, and by a change in radius due to a rate of change, $v \equiv d\ell/dt$:

$$\begin{aligned}\vec{r}' &= \vec{r} + \vec{v}dt + O(dt^2) \\ \vec{v}' &= \vec{v} + \vec{a}dt + O(dt^2) \\ \ell' &= \ell + vdt + O(dt^2)\end{aligned}\tag{1}$$

(Taylor's series about time t .) For gas bubbles in the ocean and elsewhere, the acceleration results from several influences that include gravity, buoyancy, and entrainment of bubbles by the fluid, while the rate of change of bubble radii is caused by hydrodynamic compression, surface tension and gas diffusion. Expressions for \vec{a} and v are obtained in section four where single bubble dynamics is discussed.

Conservation of bubbles demands that the number of bubbles in the volume element at time $t+dt$, $\psi(\vec{r}', \vec{v}', \ell', t+dt)d^7\tau'$, equals the number that start in the volume element at time t , $\psi(\vec{r}, \vec{v}, \ell, t)d^7\tau$, plus (minus) any bubbles that are introduced (lost) by distributed sources (sinks), $S(\vec{r}, \vec{v}, \ell, t)d^7\tau dt$:

$$\psi(\vec{r}', \vec{v}', \ell', t+dt)d^7\tau' - \psi(\vec{r}, \vec{v}, \ell, t)d^7\tau = S(\vec{r}, \vec{v}, \ell, t)d^7\tau dt + O(dt^2), \tag{2}$$

where $S(\vec{r}, \vec{v}, \ell, t)d^7\tau$ is the rate at which bubbles are introduced into $d^7\tau$ about (\vec{r}, \vec{v}, ℓ) by distributed sources. To develop equation (2) it is sufficient to note that terms of $O(dt^2)$ will disappear in the limit $dt \rightarrow 0$. Therefore we expand $\psi' \equiv \psi(\vec{r}', \vec{v}', \ell', t+dt)$ in a Taylor series about $\psi \equiv \psi(\vec{r}, \vec{v}, \ell, t)$ and keep

terms through $O(dt)$:

$$\psi' = \psi + (\partial\psi/\partial t)dt + (\vec{v} \cdot \vec{\nabla}_x \psi)dt + (\vec{a} \cdot \vec{\nabla}_v \psi)dt + v(\partial\psi/\partial \ell)dt + O(dt^2) \quad (3)$$

where $\vec{\nabla}_x(\cdot) \equiv (\partial(\cdot)/\partial x, \partial(\cdot)/\partial y, \partial(\cdot)/\partial z)$ and $\vec{\nabla}_v(\cdot) \equiv (\partial(\cdot)/\partial v_x, \partial(\cdot)/\partial v_y, \partial(\cdot)/\partial v_z)$ are Cartesian representations of the "del" operators in position space and velocity space, respectively.

To proceed, $d^7\tau'$ must be expressed in terms of $d^7\tau$:

$$d^7\tau' = \gamma(t+dt, t) d^7\tau \quad (4a)$$

where

$$\gamma(t+dt, t) \equiv \frac{\partial(\vec{r}', \vec{v}', \ell')}{\partial(\vec{r}, \vec{v}, \ell)} \equiv \det((q_j' / q_i)) \quad (4b)$$

$$i, j = 1, 2, \dots, 7$$

is the Jacobian with

$$q_1 \equiv x, q_2 \equiv y, q_3 \equiv z, q_4 \equiv v_x, q_5 \equiv v_y, q_6 \equiv v_z, \text{ and } q_7 \equiv \ell; \quad (5)$$

$$q_1' \equiv x', q_2' \equiv y', \text{ etc.}$$

The expression derived for γ in the appendix can be expanded in a Taylor series about t , or equation (1) can be used to compute the determinant in (4b) directly. In either case the result is

$$\gamma(t+dt, t) = 1 + (\vec{\nabla}_v \cdot \vec{a})dt + (v\partial/\partial \ell)dt + O(dt^2) \quad (6)$$

Substituting (3), (4) and (6) into (2), collecting terms of $O(dt)$, dividing by $d^7\tau dt$, and taking the limit $dt \rightarrow 0$, yields the bubble transport equation:

$$\partial\psi/\partial t + \vec{v} \cdot \vec{\nabla}_{\vec{r}} \psi + \vec{a} \cdot \vec{\nabla}_{\vec{v}} \psi + v \partial\psi/\partial \ell = S - \Sigma_t \psi \quad (7)$$

$$\text{where} \quad \Sigma_t \equiv \vec{\nabla}_{\vec{v}} \cdot \vec{a} + \partial v / \partial \ell \quad (8)$$

and where $-\infty < x, y, z < \infty$, $-\infty < v_x, v_y, v_z < \infty$, and $0 < \ell < \infty$.

A simpler (but less rigorous) derivation of equation (7) is obtained by recognizing that $\vec{v}\psi$, $\vec{a}\psi$, and $v\psi$ are the fluxes of bubbles in position space, velocity space, and radius space, respectively. Then

$$F \equiv - \{ \vec{\nabla}_{\vec{r}} \cdot (\vec{v}\psi) + \vec{\nabla}_{\vec{v}} \cdot (\vec{a}\psi) + \partial(v\psi)/\partial \ell \}$$

is the net flux of bubbles into $d^7\tau$ by virtue of "streaming" in seven-dimensional space, (\vec{r}, \vec{v}, ℓ) . Since the time rate of change of ψ in $d^7\tau$ is due to bubble streaming into $d^7\tau$, as well as to other sources, S , we have $\partial\psi/\partial t = F + S$. Using the identity $\vec{\nabla}_{\vec{v}} \cdot (\vec{a}\psi) = \vec{a} \cdot \vec{\nabla}_{\vec{v}} \psi + \psi \vec{\nabla}_{\vec{v}} \cdot \vec{a}$ and the fact that \vec{r} and \vec{v} are independent variables ($\vec{\nabla}_{\vec{r}} \cdot \vec{v} = 0$) yields equation (7).

The term $\Sigma_t \psi$ in the bubble transport equation is generally nonzero due to the functional dependence of acceleration, $\vec{a}(\vec{r}, \vec{v}, \ell, t)$, and radius change rate, $v(\vec{r}, \vec{v}, \ell, t)$, on the bubble velocity and radius, respectively. This is unusual since in transport equations normally encountered, the term corresponding to $\Sigma_t \psi$ is generally zero (Chapman & Cowling 1964, p.46 and p.322). Mathematically, $\Sigma_t \neq 0$ causes the volume element

$$d^7\tau' = [1 + \Sigma_t dt + O(dt^2)] d^7\tau$$

to change appreciably in the time interval dt . Physically, the term $-\Sigma_t \psi$ on the right hand side of (7) acts as a pseudo source, or sink, depending upon the functional form of \vec{a} and v .

For example, suppose \vec{a} is proportional to $(-\vec{v})$. Then $\vec{\nabla}_v \cdot \vec{a} < 0$, and the bubbles are decelerated into a smaller volume, $d^3v' = (1 + \vec{\nabla}_v \cdot \vec{a} dt) d^3v$. This increases the density so $-(\vec{\nabla}_v \cdot \vec{a})\psi$ acts like a "source" in (7). Similarly, suppose v is proportional to $v_z \ell$ so that $\partial v / \partial \ell$ is proportional to v_z . For $v_z > 0$ the bubble radii are increasing and becoming more spread out over a larger interval, $d\ell' = (1 + (\partial v / \partial \ell) dt) d\ell$. This decreases the density, so $-(\partial v / \partial \ell)\psi$ acts like a "sink" in (7).

The second term on the right hand side of (7), $S(\vec{r}, \vec{v}, \ell, t)$, represents distributed bubble sources and sinks. In addition to external sources and sinks, this term can include the effects of phenomena such as bubble scattering off small scale turbulent eddies, bubble-bubble interactions, etc. For instance, when the scale of turbulent eddies is the order of bubble radius, they will be referred to as "small scale," and bubbles entrained by the fluid may scatter off of them. To handle this phenomenon one could define a turbulent scattering cross section, Σ_s , such that

$$\Sigma_s(\vec{r}, \vec{v}_1 \rightarrow \vec{v}, \ell_1 \rightarrow \ell, t) v_1 \psi(\vec{r}, \vec{v}_1, \ell_1, t) d^3v_1 d\ell_1 d^7\tau$$

represents the probable rate at which bubbles in d^3r about \vec{r} at time t are scattered by turbulent eddies from d^3v_1 about \vec{v}_1 and $d\ell_1$ about ℓ_1 into d^3v about v and $d\ell$ about ℓ , where $v_1 = |\vec{v}_1|$ is the speed. Then

$$S(\vec{r}, \vec{v}, \ell, t) = \int \Sigma_s(\vec{r}, \vec{v}_1 \rightarrow \vec{v}, \ell_1 \rightarrow \ell, t) v_1 \psi(\vec{r}, \vec{v}_1, \ell_1, t) d^3v_1 d\ell_1$$

$$- v \psi(\vec{r}, \vec{v}, \ell, t) \int \Sigma_s(\vec{r}, \vec{v} \rightarrow \vec{v}_1, \ell \rightarrow \ell_1, t) d^3v_1 d\ell_1$$

(9)

represents the net rate at which bubbles are introduced into $d^3\tau$. Specification of Σ_s requires detailed knowledge of the turbulent field as well as a model for bubble-eddy interaction.

Substitution of equation (9) into (7) results in an integro-differential bubble transport equation. If bubble-bubble interactions are included, the bubble transport equation is nonlinear as well (Chapman and Cowling 1964, p.63). Below the surface in the upper ocean the average separation between bubbles is about 1000 times the bubble radii (Medwin 1970), but very near or at the surface wave action can cause higher bubble densities. In addition, the energy contained small scale turbulence appears to increase with wave action but to decrease with depth (Shonting 1968). To avoid at this time obvious analytical complications, the bubble density will be assumed low enough so that bubble-bubble interactions are negligible. It will also be assumed that the energy contained in small scale turbulence is negligibly small, so the bubbles are partially entrained by the fluid without abrupt changes in velocity or radius. These assumptions should be valid except very near the surface in heavy seas.

Suppose the source, $S(\vec{r}, \vec{v}, \ell, t)$, is independent of ψ or, at most, is proportional to ψ ,

$$S = S_1 + \Sigma_1 \psi \quad (10)$$

This mathematical simplification yields a linear, first order, partial differential bubble transport equation whose formal solution is outlined in the next section. It is worthwhile to note that the simplifying assumption (10) is not a severe limitation for many problems involving gas bubble transport in the upper ocean. All external bubble sources such as surface waves, rain and snow nucleation, organic decay, and photosynthesis can be included, as well as simple models of bubble scattering, absorption, and creation that have the form (10).

III. SOLUTION BY METHOD OF CHARACTERISTICS

The first order partial differential equation (7) is equivalent to the following set of eight simultaneous, first order, ordinary differential equations with initial conditions:

$$d\vec{r}/dt = \vec{v}, \quad -\infty < x, y, z < \infty, \quad \vec{r}(t_0) = \vec{r}_0 = (x_0, y_0, z_0) \quad (11a-c)$$

$$d\vec{v}/dt = \vec{a}, \quad -\infty < v_x, v_y, v_z < \infty, \quad \vec{v}(t_0) = \vec{v}_0 = (v_{x0}, v_{y0}, v_{z0}) \quad (11d-f)$$

$$d\ell/dt = v, \quad 0 \leq \ell < \infty, \quad \ell(t_0) = \ell_0 \quad (11g)$$

$$d\psi/dt = S - \Sigma_t \psi, \quad 0 \leq \psi < \infty, \quad \psi(t_0) = \psi_0 \quad (12)$$

The equivalence between these "characteristic equations" and the bubble transport equation is most lucidly demonstrated with a geometric argument given by Garabedian (1964, p.18). The parametrically-represented curve C in nine-dimensional space,

$$\vec{R}(t) \equiv [t, x(t), y(t), z(t), v_x(t), v_y(t), v_z(t), \ell(t), \psi(t)], \quad -\infty < t < \infty,$$

obtained by integrating the characteristic equations (11) and (12), is called a "characteristic curve." Components of the initial point, $\vec{R}(t_0)$, are called "characteristics." The family of characteristic curves,

$$\{\vec{R}(t) : -\infty < t < \infty, \vec{R}(t_0) \in \mathcal{F}\},$$

parameterized by the set \mathcal{F} of accessible characteristics, forms a hypersurface in nine-dimensional space, $\psi(t; \vec{r}_0, \vec{v}_0, \ell_0, t_0)$, that satisfies the bubble transport equation.

The family of characteristic curves is essentially parameterized by the set $(\vec{r}_0, \vec{v}_0, \ell_0)$ of accessible initial conditions since t_0 and $\psi_0(\vec{r}_0, \vec{v}_0, \ell_0)$, the initial distribution, are generally fixed for a given problem. Since \vec{a} , v ,

and S are generally functions of \vec{r}, \vec{v}, ℓ , and t , the solutions to (11) and (12) are not only functions of the parameter t , but they also depend upon all the initial conditions $(\vec{r}_0, \vec{v}_0, \ell_0)$:

$$\vec{r} = \vec{r}(t; \vec{r}_0, \vec{v}_0, \ell_0, t_0) \equiv \vec{r}(t) \quad (13a)$$

$$\vec{v} = \vec{v}(t; \vec{r}_0, \vec{v}_0, \ell_0, t_0) \equiv \vec{v}(t) \quad (13b)$$

$$\ell = \ell(t; \vec{r}_0, \vec{v}_0, \ell_0, t_0) \equiv \ell(t) \quad (13c)$$

$$\text{and } \psi = \psi(t; \vec{r}_0, \vec{v}_0, \ell_0, t_0) \equiv \psi(t) \quad (13d)$$

where the short notation on the right is used for brevity.

The characteristic equations (11) are simply the bubble dynamics equations. The bubble dynamics model used to construct \vec{a} and ν (see §4), as well as the characteristics $(\vec{r}_0, \vec{v}_0, \ell_0)$, determine a "trajectory" $(\vec{r}(t), \vec{v}(t), \ell(t))$ which is the projection of a characteristic curve from nine-dimensional space onto seven-dimensional space. Bubble trajectories in (x, y, z) space are likewise projections of characteristic curves.

A. Lagrangian and Eulerian Representations

The parametric representation (13), obtained by integrating the characteristic equations simultaneously, describes the continuum from a Lagrangian frame of reference. In this description, bubbles are labeled by group according to their characteristics $(\vec{r}_0, \vec{v}_0, \ell_0)$. This moving frame follows a specific group, initially in $d^7\tau_0 = d^3r_0 d^3v_0 d\ell_0$ about $(\vec{r}_0, \vec{v}_0, \ell_0)$ at t_0 , along a characteristic curve to $d^7\tau(t)$ about $(\vec{r}(t), \vec{v}(t), \ell(t))$ at t . At any time t , $\psi(t)d^7\tau(t)$ is the number of bubbles, belonging to the group labeled $(\vec{r}_0, \vec{v}_0, \ell_0)$, that are found in $d^7\tau(t)$ about $(\vec{r}(t), \vec{v}(t), \ell(t))$.

III. SOLUTION BY METHOD OF CHARACTERISTICS

The first order partial differential equation (7) is equivalent to the following set of eight simultaneous, first order, ordinary differential equations with initial conditions:

$$d\vec{r}/dt = \vec{v}, \quad -\infty < x, y, z < \infty, \quad \vec{r}(t_0) = \vec{r}_0 = (x_0, y_0, z_0) \quad (11a-c)$$

$$d\vec{v}/dt = \vec{a}, \quad -\infty < v_x, v_y, v_z < \infty, \quad \vec{v}(t_0) = \vec{v}_0 = (v_{x0}, v_{y0}, v_{z0}) \quad (11d-f)$$

$$d\ell/dt = v, \quad 0 \leq \ell < \infty, \quad \ell(t_0) = \ell_0 \quad (11g)$$

$$d\psi/dt = S - \Sigma_t \psi, \quad 0 \leq \psi < \infty, \quad \psi(t_0) = \psi_0 \quad (12)$$

The equivalence between these "characteristic equations" and the bubble transport equation is most lucidly demonstrated with a geometric argument given by Garabedian (1964, p.18). The parametrically-represented curve C in nine-dimensional space,

$$\vec{R}(t) \equiv [t, x(t), y(t), z(t), v_x(t), v_y(t), v_z(t), \ell(t), \psi(t)], \quad -\infty < t < \infty,$$

obtained by integrating the characteristic equations (11) and (12), is called a "characteristic curve." Components of the initial point, $\vec{R}(t_0)$, are called "characteristics." The family of characteristic curves,

$$\{\vec{R}(t) : -\infty < t < \infty, \vec{R}(t_0) \in \mathcal{F}\},$$

parameterized by the set \mathcal{F} of accessible characteristics, forms a hypersurface

in nine-dimensional space, $\psi(t; \vec{r}_0, \vec{v}_0, \ell_0, t_0)$, that satisfies the bubble transport equation.

The family of characteristic curves is essentially parameterized by the set $(\vec{r}_0, \vec{v}_0, \ell_0)$ of accessible initial conditions since t_0 and $\psi_0(\vec{r}_0, \vec{v}_0, \ell_0)$, the initial distribution, are generally fixed for a given problem. Since \vec{a} , v ,

and S are generally functions of \vec{r}, \vec{v}, ℓ , and t , the solutions to (11) and (12) are not only functions of the parameter t , but they also depend upon all the initial conditions $(\vec{r}_0, \vec{v}_0, \ell_0)$:

$$\vec{r} = \vec{r}(t; \vec{r}_0, \vec{v}_0, \ell_0, t_0) \equiv \vec{r}(t) \quad (13a)$$

$$\vec{v} = \vec{v}(t; \vec{r}_0, \vec{v}_0, \ell_0, t_0) \equiv \vec{v}(t) \quad (13b)$$

$$\ell = \ell(t; \vec{r}_0, \vec{v}_0, \ell_0, t_0) \equiv \ell(t) \quad (13c)$$

$$\text{and } \psi = \psi(t; \vec{r}_0, \vec{v}_0, \ell_0, t_0) \equiv \psi(t) \quad (13d)$$

where the short notation on the right is used for brevity.

The characteristic equations (11) are simply the bubble dynamics equations. The bubble dynamics model used to construct \vec{a} and \vec{v} (see §4), as well as the characteristics $(\vec{r}_0, \vec{v}_0, \ell_0)$, determine a "trajectory" $(\vec{r}(t), \vec{v}(t), \ell(t))$ which is the projection of a characteristic curve from nine-dimensional space onto seven-dimensional space. Bubble trajectories in (x, y, z) space are likewise projections of characteristic curves.

A. Lagrangian and Eulerian Representations

The parametric representation (13), obtained by integrating the characteristic equations simultaneously, describes the continuum from a Lagrangian frame of reference. In this description, bubbles are labeled by group according to their characteristics $(\vec{r}_0, \vec{v}_0, \ell_0)$. This moving frame follows a specific group, initially in $d^7\tau_0 = d^3r_0 d^3v_0 d\ell_0$ about $(\vec{r}_0, \vec{v}_0, \ell_0)$ at t_0 , along a characteristic curve to $d^7\tau(t)$ about $(\vec{r}(t), \vec{v}(t), \ell(t))$ at t . At any time t , $\psi(t)d^7\tau(t)$ is the number of bubbles, belonging to the group labeled $(\vec{r}_0, \vec{v}_0, \ell_0)$, that are found in $d^7\tau(t)$ about $(\vec{r}(t), \vec{v}(t), \ell(t))$.

On the other hand, the distribution $\psi(\vec{r}, \vec{v}, \ell, t)$, expressed with \vec{r}, \vec{v}, ℓ , and t as independent variables, more conveniently describes the continuum from an Eulerian viewpoint. The Eulerian frame is fixed, and attention is focused on the particular volume $d^7\tau$ about the point (\vec{r}, \vec{v}, ℓ) . The instantaneous bubble density $\psi(\vec{r}, \vec{v}, \ell, t)d^7\tau$ is considered without regard to the characteristics of bubbles in the volume.

B. Formal Solution

If the source, $S(\vec{r}, \vec{v}, \ell, t)$, has the form (10), then (7) is analogous to the Boltzmann transport equation written for neutral particles (e.g., photons or neutrons) or charged particles (e.g., electrons) in a purely absorbing medium with distributed sources (Case and Zweifel 1967, p.31 and p.247). For example, neutrons will stream along their characteristic curves in (x, y, z) space, which are straight lines, until they are absorbed or until they escape the medium. Similarly, the bubbles described by (7) stream along their characteristic curves in (\vec{r}, \vec{v}, ℓ) space until they disappear ($\ell \rightarrow 0$) or until they escape the medium. However, the characteristic curves defined by (11) are generally not straight lines in (\vec{r}, \vec{v}, ℓ) space or any of its subspaces, such as (x, y, z) .

With S given by (10), the formal solution to (7) is obtained by integrating (12):

$$\begin{aligned} \psi(t; \vec{r}_0, \vec{v}_0, \ell_0, t_0) &= \psi(\vec{r}_0, \vec{v}_0, \ell_0, t_0) \exp[T_1(t, t_0) - T_2(t, t_0)] \\ &+ \int_{t_0}^t S_1(\vec{r}(t'), \vec{v}(t'), \ell(t'), t') \exp[T_1(t, t') - T_2(t, t')] dt' \end{aligned} \quad (14)$$

where

$$T_1(t, t_0) \equiv \int_{t_0}^t \Sigma_1(\vec{r}(t'), \vec{v}(t'), \ell(t'), t') dt'$$

and

$$T_2(t, t_0) \equiv \int_{t_0}^t \Sigma_t(\vec{r}(t'), \vec{v}(t'), \ell(t'), t') dt'.$$

All integrals in this expression, and all similar integrals appearing elsewhere in this paper, are understood to be line integrals along the characteristic curve that passes through $(\vec{r}_0, \vec{v}_0, \ell_0)$ and (r, v, ℓ) .

To obtain the number of bubbles in $d^7\tau$ about (\vec{r}, \vec{v}, ℓ) at time t , (14) is multiplied by this volume element. However, a consistent representation for the right hand side of the equation requires use of the Jacobian,

$$\gamma(t, t') \equiv \partial(\vec{r}(t), \vec{v}(t), \ell(t)) / \partial(\vec{r}(t'), \vec{v}(t'), \ell(t')),$$

which transforms the volume element from one point to another on the same characteristic curve:

$$d^7\tau = \gamma(t, t') d^7\tau'.$$

Using the expression derived in the appendix,

$$\gamma(t, t') = \exp[T_2(t, t')], \quad (15)$$

the solution can be rewritten in the convenient form

$$\begin{aligned} \psi(\vec{r}, \vec{v}, \ell, t) d^7\tau &= \exp[T_1(t, t_0)] \psi(\vec{r}_0, \vec{v}_0, \ell_0, t_0) d^7\tau_0 \\ &+ \int_{t_0}^t \exp[T_1(t, t')] S_1(\vec{r}', \vec{v}', \ell', t') d^7\tau' dt', \end{aligned} \quad (16)$$

where the abbreviations $\vec{r} = \vec{r}(t; \vec{r}_0, \vec{v}_0, \ell_0, t_0)$, $\vec{r}' = \vec{r}(t'; \vec{r}_0, \vec{v}_0, \ell_0, t_0)$, etc., have been used. From this expression it is apparent that the number of bubbles in $d^7\tau$ about (\vec{r}, \vec{v}, ℓ) at time t is a sum along the characteristic curve that passes through (\vec{r}, \vec{v}, ℓ) at t . It is the number originally in $d^7\tau_0$ about $(\vec{r}_0, \vec{v}_0, \ell_0)$ at t_0 plus (minus) those added (subtracted) by sources (sinks) along the characteristic curve between $(\vec{r}_0, \vec{v}_0, \ell_0)$ and (\vec{r}, \vec{v}, ℓ) . If $\Sigma_1 \neq 0$ in (10) then the result is amplified (attenuated) by the factors $\exp[T_1]$ because of the creation (absorption) rate $\Sigma_1 \psi$ along the path. For $t = t_0 + dt$, (16) expanded in a Taylor series to $O(dt)$ yields equation (2), as it must.

Equations (7) and (16) are equivalent statements about the physical model outlined at the beginning of section two. They formally represent relationships that exist between the bubble distribution, single bubble dynamics, and the bubble sources. As such, these equations can be used for calculations to investigate relationships among the three in real situations. For example, if any two are specified, properties of the third can be inferred, either directly or indirectly.

Prior to using (16) for calculations, a bubble dynamics model (\vec{a} & v) must be specified so that equations (11) can be integrated to obtain the characteristic curves. A fair amount of information is available concerning single bubble dynamics, and in the next section some of the important points are summarized.

The distributed sources and fluid properties, as well as the appropriate bubble dynamics model, are dependent on the particular situation being analyzed. In section five the problem of gas bubble transport in the upper ocean is used as the basis for some general remarks concerning bubble sources and fluid velocity fields. Then equations (7) and (16) are written for a simple ocean model, and some calculations are performed to demonstrate how (16) can be used to evaluate the bubble distribution when the source function and bubble dynamics have been specific.

It is significant to note that both (14) and (16) represent the distribution from a Lagrangian view point, $\psi(t; \vec{r}_0, \vec{v}_0, l_0, t_0)$. Transformation to the more convenient Eulerian expression, $\psi(\vec{r}, \vec{v}, l, t)$, requires the inverse of equations (13), namely $\vec{r}_0(t_0; \vec{r}, \vec{v}, l, t)$, $\vec{v}_0(t_0; \vec{r}, \vec{v}, l, t)$, and $l_0(t_0; \vec{r}, \vec{v}, l, t)$. In general, equations (11) will have to be integrated numerically to establish a mapping between $(\vec{r}_0, \vec{v}_0, l_0, t_0)$ and (\vec{r}, \vec{v}, l, t) , but often approximations can be made that will yield analytical expressions.

If S is a more complicated function of ψ than (10), the formal solution (16) represents an integral equation for ψ . When analytical methods aimed at solving (7) or (16) fail, the Neumann series solution to the integral equation can be used to generate numerical results, if the series converges fast enough.

IV. SINGLE BUBBLE DYNAMICS

In this section general expressions are derived for \vec{a} and v , and some known models of gas diffusion and drag are summarized for gas bubbles in liquids. For the purpose of discussion in sections four and five, consider an inertial cartesian coordinate system with the z-axis vertical upward and the origin at the surface of the liquid. Let \vec{v} be the bubble velocity and $\vec{V}(\vec{r}, t)$ be the transporting fluid's velocity relative to this frame of reference.

A. Acceleration

If a bubble of volume σ , containing fluid of density ρ , were completely entrained ($\vec{v} = \vec{V}$) by a fluid of density ρ_0 , it would experience the same force, $\rho_0 \sigma d\vec{V}/dt$, as would transporting fluid enclosed in the same volume. For $\rho \neq \rho_0$, partial entrainment occurs, and the bubble maintains a relative velocity, $\vec{u} \equiv \vec{v} - \vec{V}$, with respect to the transporting fluid. Hence, the bubble experiences a drag force, \vec{F}_D , which is discussed shortly in the context of gas bubbles in liquids.

As the bubble moves relative to the transporting fluid it "drags" with it an amount of fluid having a volume equal to some fraction, β , of the bubble volume. By Newton's third law, this adhering mass provides a supplemental reaction term, $-(\beta \sigma \rho_0 d\vec{u}/dt)$, that acts to increase the bubble's effective inertial mass. In addition, there is a net buoyant force, $\sigma g(\rho_0 - \rho)\hat{k}$, where \hat{k} is a unit vector vertically upward and g is the acceleration of gravity. Combining all of these forces in Newton's second law yields the following expression for acceleration:

$$\begin{aligned} \vec{a} = & \vec{F}_D / (\sigma \rho_0 (\beta + \rho / \rho_0)) + (1 + \beta) (d\vec{V}/dt) / (\beta + \rho / \rho_0) \\ & + (1 - \rho / \rho_0) g \hat{k} / (\beta + \rho / \rho_0) \end{aligned} \quad (17)$$

in which

$$d\vec{V}/dt = \partial\vec{V}/\partial t + (\vec{V} \cdot \nabla_r) \vec{V} \quad (18)$$

B. Drag on Gas Bubbles in a Liquid

Because of its theoretical and practical importance, the motion of gas bubbles in liquids (e.g., air bubbles in water) has been actively studied (Levich 1962, §80). The regimes of bubble motion are classified according to Reynold's number, $R_e = u_0 \ell / \eta$, where η is the liquid's viscosity. Observations of different-size bubbles rising in various liquids indicate that small ($R_e < 1$) and medium-size ($1 < R_e < 700$) bubbles maintain a spherical shape, whereas large ($R_e > 700$) bubbles deform to flattened ellipsoids and very large bubbles ($R_e > 4500$) are unstable and tend to break up.

For small bubbles ($\ell \lesssim 100\mu \approx 10^{-4}\text{m}$ in water) the drag is viscous in nature and is given by

$$\vec{F}_V = - \kappa \eta \ell \vec{u}, \quad (19)$$

with $\kappa = 4\pi$ for a perfectly clean bubble having a mobile two fluid interface at its surface. However, most liquids such as water contain "surface-active" materials that coat the bubble and destroy the mobility of this interface. In this case the relative velocity of the transporting fluid goes to zero at the bubble's surface, and the bubble behaves like a solid sphere where drag is given by (19) with $\kappa = 6\pi$ (Levich 1962, §§ 70 and 81).

The flow past medium-size bubbles ($100\mu \lesssim \ell \lesssim 2000\mu$ in water) is separated, with the separation region occupying an area s_1 on the downstream portion of the bubble's surface. Up to the separation point resistance that acts on the bubble is viscous in nature with a contribution to the total drag given by (19)

with $\kappa = 12\pi$. Past the separation point and into the bubble's wake the flow is characterized by turbulent motion with a contribution to the total drag given by

$$\vec{F}_T = -0.5K_f \rho s_1 u \vec{u}, \quad (20)$$

where K_f is a drag coefficient with $0.65 > K_f > 0.55$ for $200 < R_e < 1000$ (Levich 1962, §§ 80 and 82).

In the absence of surface active materials, s_1 is very small ($s_1 \sim \ell^2/R_e$ for $R_e \gg 1$), so flow past the bubble is essentially unseparated and the drag is given by (19) with $\kappa = 12\pi$. On the other hand, when an area s_0 on the bubble is covered by a monolayer of surface-active material, the relative fluid velocity in this region is zero, and flow separation occurs there. In this case viscous drag (19) is accompanied by the form drag (20) with $s_1 = s_0$, and the latter dominates the former when

$$s_0/(4\pi\ell^2) > 28(\eta/\rho_0)^2/(g\ell^3)$$

(Levich 1962, § 82). For example, when $\ell = 500\mu$, only 2% of the bubble's surface need be covered by a monolayer of this material before the drag force becomes quadratic according to (20).

C. Radius Change Rate

For gas bubbles moving in a liquid such as water, radius changes are caused primarily by changes in pressure, due to changes in depth or surface tension, or by gas diffusion across the bubble surface. Spherical bubbles ($R_e < 700$) that contain n moles of ideal gas at temperature T and pressure P are described by

$$4\pi\ell^3/3 = nRT/P, \quad (21)$$

where R is the gas constant. For isothermal processes, (21) is readily differentiated to yield

$$v = \frac{d\ell}{dt} = \frac{\ell}{3} \left(\frac{dn/dt}{n} - \frac{dP/dt}{P} \right). \quad (22)$$

Gas diffusion is included in the dn/dt term, while compression and surface tension are included in dP/dt . Assuming quasi-equilibrium, gas pressure is the sum of atmospheric pressure, P_0 , surface tension pressure, $2\zeta/\ell$, and fluid weight, $-\rho_0 g z$, where $-z \geq 0$ is the depth and ζ is the surface tension:

$$P = P_0 - \rho_0 g z + 2\zeta/\ell, \quad (23)$$

and

$$dP/dt = -\rho_0 g v_z - (2\zeta/\ell^2) d\ell/dt. \quad (24)$$

D. Gas Diffusion

As results of the next section will indicate, gas diffusion is one of the more important factors affecting the bubble distribution. It is a complex phenomenon depending upon many influences that include the type of gas in the bubble, the gas diffusivity, D , in the transporting liquid, the gas concentration, C , in liquid contacting the bubble's surface, the gas concentration, C_∞ , in liquid far away from the bubble, the presence of surface-active materials in the liquid and on the surface of the bubble, the flow field around the bubble and the bubble radius. To simplify the discussion here it will be assumed that gas inside the bubble is composed of one type of "average" molecule having a single diffusivity, D .

If the Péclet number is large, $P_e \equiv (u\ell/D) \gg 1$, the gas concentration gradient is confined to a thin boundary layer on the surface of the bubble, and diffusion between C and C_∞ occurs across a small distance $d \sim \ell/P_e^{1/2}$. Hence (Levich 1962, §§ 14 and 72)

$$dn/dt = -G\ell^2(C-C_\infty), \quad (25)$$

where the coefficient G is generally a function of ℓ , u , and D . For specific applications in which individual components of gas must be monitored, equation (25) will have to be generalized.

Typically $(\eta/\rho)/D \sim 10^3$, so there is a wide range of bubble radii for which the Péclet number is large ($Pe > 1$) but the Reynold's number is small ($Re < 1$). For that case (small bubbles),

$$G = 3[(\pi/6)(Du/\ell)]^{1/2} \quad (26)$$

in the absence of surface-active material (Levich 1962, §§ 72 and 91). In the presence of surface-active material, the flow field around a small bubble is like that around a solid sphere, and G becomes (Levich 1962, § 14)

$$G = 8(D^2u/\ell^2)^{1/3} \quad (27)$$

A representative value for u is the terminal speed, u_T , of small bubbles rising in a quiescent fluid. Equating the drag (19) to the buoyant force, $4\pi\ell^3g\rho_0/3$, which assumes $\rho/\rho_0 < 1$, results in the expression

$$u_T = (4\pi/3\kappa)(g\rho_0\ell^2/\eta) \quad (28)$$

where $\kappa = 4\pi$ in the absence of surface-active materials, and $\kappa = 6\pi$ in their presence.

At moderate Reynold's numbers (medium-size bubbles) the flow is separated, but the region of separation, s_1 , is generally small. If gas diffusion across s_1 can be neglected, (25) represents the gas diffusion with G equal to (26) multiplied by $\sqrt{3}$ (Levich 1962, § 91).

If liquid in contact with the bubble surface is assumed to always be saturated with gas at the pressure P (in atmospheres) prevailing inside the bubble, then $C = KP$, where K is the absorption coefficient ($\text{kg}\cdot\text{m}^{-3}\cdot\text{atm}^{-1}$) for the liquid-gas system. Defining the partial pressure $f \equiv C_\infty/K$ (in atm) of gas in the transporting fluid, (25) can be rewritten

$$dn/dt = -GK\ell^2(P-f). \quad (29)$$

Under laboratory conditions, Wyman, et al (1952), measured the rate of solution and the change in composition of air bubbles in stirred sea water, as a function of depth. These experimental results follow very closely

$$dn/dt = -4\pi\delta\ell^2(P-f) \quad (30)$$

with $\delta \cong 4.4 \times 10^{-5} \text{ moles m}^{-2}\text{sec}^{-1}\text{atm}^{-1}$. Using equations (26) and (27) with published values of D and K for oxygen and nitrogen in water, estimates of GK are found comparable to $4\pi\delta$, but generally larger. The presence of surface-active materials that retard gas diffusion and reduce the effective absorption coefficient across the bubble's surface may have contributed to the discrepancy (Fox & Herzfeld 1954).

V. APPLICATION TO THE UPPER OCEAN

The purpose of this section is to briefly discuss application of bubble transport theory to the description of gas bubble populations in the upper ocean. Because it involves a variety of interrelated phenomena pertaining to different disciplines, this is a difficult subject to analyze. Also, there is only limited information available upon which to base mathematical models of bubble sources, fluid velocity fields, gas diffusion rates, etc. However, it is the author's opinion that bubble transport theory is a useful tool for interpreting data and relating phenomena that affect the distribution.

To begin, it is appropriate to summarize some observations concerning bubble sources, S , and fluid velocity fields, \vec{V} , in the upper ocean and to make a few remarks concerning analysis. Then, to demonstrate an application of bubble transport theory, some sample calculations are performed and interpreted.

A. Bubble Sources and Fluid Velocity Fields

Physically one might consider bubble sources to be segregated into three categories according to depth: Those on the ocean floor, those concentrated at the surface, and those distributed throughout the medium, principally near the surface. Mathematically these classifications are convenient for analysis since sources in the first two categories can be incorporated into (7) and (16) either as boundary conditions or as plane sources.

The first category includes sediment-initiated bubbles which often contain organic gas. For example, McCartney and Bary (1965) measured relatively large bubbles with radii between 450μ and 800μ coming off the bottom of Saanich Inlet, British Columbia, and speculated that these bubbles contained methane.

In the second category are bubbles generated at or very near the surface by wind and wave action, precipitation, and captured aerosols. The subsurface measurements of Blanchard and Woodcock (1957), Glotov, et al (1962), and Medwin (1970) imply that most of the bubbles associated with breaking waves have radii less than 200μ . On the other hand, experiments conducted by Monahan and Zietlow (1969), in which a small volume of seawater was poured into a tank of the same, indicate that the cloud of bubbles formed by the descending plume of mixed air and water contains an appreciable number of 200μ to 1000μ bubbles as well. In addition to wave-generated bubbles, rain and snow nucleate bubbles at the surface which have radii predominantly less than 50μ (Blanchard and Woodcock 1957). To explain the excessive sound attenuation and scatter observed in near-surface water at high frequencies ($f > 60\text{kHz}$), Medwin (1970) speculated that continental aerosols may be the primary source of small bubbles ($\ell < 50\mu$) near the surface.

In the third category are bubbles initiated within the volume of the upper ocean. Internal wave action, radiation, and biological activity, such as photosynthesis and marine life gas emissions, have been postulated to be responsible for many of the smallest bubbles ($\ell \sim 60\mu$). Also, some of the volume sources may be associated with pressure fluctuations caused by wind-driven surface waves. Pressure changes and turbulence may nucleate small bubbles at distributed cavitation sites, while the vertical fluid velocity and turbulence created by breaking waves introduces larger bubbles below the surface.

When a wave breaks and air is rapidly mixed with water, the bubbles formed are entrained by a strong vertical velocity field; these bubbles have been observed as far as three wave heights below the surface (Kanwisher 1963). As the strong downward currents decay, the bubbles tend to rise under buoyancy with motion modified by the remaining fluid velocity field (ref. equation (17)).

The largest bubbles rise most quickly and reach the surface before going into solution while the smallest bubbles succumb to gas diffusion (LeBlond 1969). As a result, the most prevalent bubble within a few meters of the surface should have a radius between the two extremes, an assertion supported by the data of Medwin (1970) and Glotov, et al (1962) who measure distribution maxima at 90 μ and 60 μ , respectively.

Shonting (1968) has measured the autospectra of particle motions in the upper ocean and shown that the dominant peaks are associated with the frequencies of the surface waves. The spectral energy decays exponentially with depth in a way that attenuates high frequencies the most rapidly.

B. Example

Consider a one-dimensional, steady state ocean in which all velocities are vertical and in which all functions depend spatially on depth only. In this case the bubble transport equation reduces to

$$v \frac{\partial \phi}{\partial z} + a \frac{\partial \phi}{\partial v} + v \frac{\partial \phi}{\partial \ell} = - \Sigma_t \phi + S, \quad (31)$$

where $\phi(z, v, \ell)$ is the distribution function, $S(z, v, \ell)$ is the distributed source, $v_z = v$ is the vertical velocity, $a_z = a(z, v, \ell)$ is the vertical acceleration, $v(z, v, \ell)$ is the radius change rate, and $\Sigma_t = \partial a / \partial v + \partial v / \partial \ell$.

The characteristic equations for (31) can be written with $z \leq 0$ chosen as the independent parameter. This choice is equivalent to dividing equations (11) and (12) by (11c):

$$dv/dz = a(z, v, \ell)/v, \quad -\infty < v < \infty \quad \& \quad v(z_0) = v_0; \quad (32a)$$

$$d\ell/dz = v(z, v, \ell)/v, \quad 0 \leq \ell < \infty \quad \& \quad \ell(z_0) = \ell_0; \quad (32b)$$

$$d\phi/dz + (\Sigma_t/v)\phi = S(z, v, \ell)/v, \quad 0 \leq \phi < \infty \quad \& \quad \phi(z_0) = \phi_0(v_0, \ell_0) \quad (33)$$

Simultaneous integration of equations (32) yields the family of characteristic curves

$$\{z, v(z; z_0, v_0, \ell_0), \ell(z; z_0, v_0, \ell_0); z \leq 0\} \quad (34)$$

and bubble trajectories in (x, y, z) space are vertical straight lines.

A formal solution analogous to (14) is readily obtained by integrating (33) along characteristic curves (34). The form analogous to (16),

$$v\phi(z, v, \ell)dv d\ell = v_0\phi(z_0, v_0, \ell_0)dv_0 d\ell_0 + \int_{z_0}^z S(z', v', \ell')dz' dv' d\ell', \quad (35)$$

is derived using the Jacobian,

$$\tilde{\gamma}(z, z') = \frac{\partial(v, \ell)}{\partial(v', \ell')} = \frac{v'}{v} \exp \left[\int_{z'}^z \Sigma_t(z'', v'', \ell'')dz''/v'' \right]. \quad (36)$$

Expression (36) follows from the differential equation

$$d\tilde{\gamma}/dz = (\Sigma_t - (a/v^2))\tilde{\gamma} \quad (37)$$

obtained when characteristic equations (32) are combined in a manner similar to the general scheme detailed in the appendix. Of course, all integrals appearing in this section are taken along characteristic curves (34), where abbreviated notation $v' \equiv v(z'; z_0, v_0, \ell_0)$, $\ell'' \equiv \ell(z''; z_0, v_0, \ell_0)$, etc. has been used in (35) and (36).

Physically equation (35) states that the flux of bubbles, $v\phi$, at the point (z, v, ℓ) , equals the flux of bubbles, $v_0\phi_0$, at the point (z_0, v_0, ℓ_0) , plus (minus) the bubbles added (removed) by distributed sources (sinks) along characteristic curve (34). Further physical insight can be gained by reflecting on a situation where there are no distributed sources, $S = 0$, so that $\phi(z; z_0, v_0, \ell_0)dv d\ell = (v_0/v)\phi(z_0, v_0, \ell_0)dv_0 d\ell_0$. If there is no fluid velocity, bubbles rise under buoyancy at terminal velocity and may shrink and slow down or expand and speed

up (LeBlond 1969). Those belonging to the Lagrangian group (z_0, v_0, ℓ_0) whose velocity and radii increase with z have a density that decreases as z increases because the bubbles at $z + dz$ are running away from those at z . On the other hand, those whose velocity and radii decrease as z increases have a density increasing with z since the bubbles at z are piling up on those at $z + dz$.

1. Characteristic Curves

A first step toward using (35) to calculate the bubble distribution is the specification of $a(z, v, \ell)$ and $v(z, v, \ell)$ and the computation of characteristic curves (34). A useful expression for the radius change rate is obtained by substituting (21), (23), (24), and (29) into (22) and solving for $d\ell/dt$. Then (32b) becomes

$$d\ell/dz = v/v = \{(\ell/3) - (GK/4\pi)(RT)[D(1-f) - z + (\Gamma/\ell)]/v\} / [D - z + (2/3)(\Gamma/\ell)] \quad (38)$$

where $(-z)$ is the depth, f is the partial pressure (in atmospheres) of gas in the water,

$$D \equiv P_0 / \rho_0 g \approx 10 \text{ meters}$$

is the depth of sea water equivalent to one atmosphere, and

$$\Gamma \equiv 2\zeta / \rho_0 g \approx 1.47 \times 10^{-5} \text{ meters}^2$$

is a surface tension coefficient in water. Note that the Γ/ℓ terms are negligible unless the bubbles are very small ($\ell \lesssim 30\mu$).

Acceleration is given by (17) with the drag force given by (19) or (20). If the fluid velocity is negligible ($\vec{V} \approx 0$), the bubbles rise very nearly at their terminal velocity, v_{T1} . This is seen in Figure 1 which was obtained by simultaneously integrating equations (32) numerically* for bubbles of various initial radii, ℓ_0 , starting from rest at $z_0 \approx -20$ meters. Small bubbles ($\ell < 100\mu$), and medium-size bubbles ($100\mu < \ell < 2000\mu$) with viscous drag dominant, rise at terminal velocity v_{T1} given approximately by equating (19) to the buoyant force:

$$v_{T1} = (g/(\kappa'\alpha))\ell^2 \quad (39)$$

where $\kappa' = 1$ and $\kappa' = 2$, respectively, and where

$$\alpha \equiv (9/2)(\eta/\rho_0) \approx 4.37 \times 10^{-6} \text{ meters}^2/\text{sec}$$

in water. When medium-size bubbles have a sufficient fraction of their surface,

$$\epsilon \equiv s_0/(4\pi\ell^2),$$

covered by a monolayer of surface active material, turbulent drag dominates viscous drag because flow separation occurs at the boundary of s_0 . They rise at terminal velocity v_{T2} given approximately by equating (20) to the buoyant force:

$$v_{T2} = (g/\xi)^{1/2}\ell^{1/2} \quad (40)$$

where

$$\xi \equiv (3/2)K_f \epsilon \approx 0.9\epsilon.$$

*All numerical integrations alluded to in this section were carried out using gaussian quadrature or optimal fourth rank Runge-Kutta (Ceschino and Kuntzmann 1966, p. 67).

Datta, et al, (1950) has averaged the results of several different observers to produce an empirical curve for the terminal velocity of air bubbles in water as a function of their radii. Values produced by (40) agree with this empirical data for $300\mu < \ell < 1000\mu$ if the surface fraction, ϵ , is reduced monotonically as the radius, ℓ , increases. This leads one to speculate that as the radius and terminal velocity increase, rapid liquid motion at the surface either washes away surface active molecules or carries them to the rear where they form a compact, saturated monolayer (Levich 1962, p.447).

In general the terminal velocity of a rising bubble is not given simply by (39) or (40) during its entire lifetime. Many bubbles shrink or expand as they rise (LeBlond 1969) and thereby transition from the regime of predominantly turbulent drag to the regime of predominantly viscous drag, or vice-versa. The treatment of separated flow in Levich (1962, § 82) suggests that the sum of (19) and (20) should be a useful model for the drag on medium-size bubbles in the transition region. Using this model in (17), (32a) can be written

$$dv/dz = -[(\xi/\beta)/\ell] [(v-v_-)(v+v_+)/v], \quad (41)$$

where

$$v_{\pm} \equiv v_{T2} [\pm 1 + (1+4Q^2)^{1/2}] / (2Q) \quad (42)$$

with

$$Q \equiv v_{T1}/v_{T2} = (\ell/\tilde{\ell})^{3/2}$$

and

$$\tilde{\ell} \equiv [(\kappa'\alpha)^2/(g\xi)]^{1/3}$$

Numerical integration of (38) and (41) demonstrates that the bubbles released from rest rise with terminal velocity $v_T = v_-$ (figure 1). This approach appears to have some merit since (42) for v_- yields values close to the empirical curve

by Datta, et al (1950) and since the model shows the proper limiting behavior:

For $\ell < \tilde{\ell}$, viscous drag dominates turbulent drag in (41) and

$$v_- = v_{T1} - v_{T1} \{Q^2 + O(Q^4)\}$$

for $\ell > \tilde{\ell}$, turbulent drag dominates in (41) and

$$v_- = v_{T2} + v_{T2} \{0.5Q^{-1} + O(Q^{-2})\}.$$

Computation of characteristic curves (34) in a quiescent fluid ($\vec{V} = 0$) is simplified because the bubble velocity is always very nearly the terminal velocity, $v = v_T(z; z_0, \ell_0)$, and is essentially independent of v_0 . Either (39), (40), (42), or empirical values for v_T can be used in (38) to obtain $\ell(z; z_0, \ell_0)$. If (39) or (40) is used and surface tension is neglected, closed analytical expressions result: For $v = v_{T1}$, $\Gamma = 0$, and f constant,

$$\ell = \ell_{T1}(z; z_0, \ell_0) = \left\{ \left(\frac{D-z_0}{D-z} \right) \ell_0^3 + \frac{3}{2} \frac{(GK/4\pi) R \Gamma}{(g/\kappa) \alpha} [(z^2 - z_0^2) - 2D(1-f)(z-z_0)] \right\}^{1/3}, \quad (43a)$$

with an inverse transformation

$$\ell_0 = \ell_{T1}(z_0; z, \ell); \quad (43b)$$

for $v = v_{T2}$, $\Gamma = 0$ and f constant,

$$\ell = \ell_{T2}(z; z_0, \ell_0) = \left\{ \left(\frac{D-z_0}{D-z} \right)^{1/2} \ell_0^{3/2} + \frac{(GK/4\pi) R \Gamma}{(g/\xi)^{1/2}} [(D-z) \left[1 - \left(\frac{D-z_0}{D-z} \right)^{3/2} \right] - 3D(2-f) \left[1 - \left(\frac{D-z_0}{D-z} \right)^{1/2} \right]] \right\}^{2/3} \quad (44a)$$

with an inverse transformation

$$\ell_o = \ell_{T2}(z_o; z, \ell). \quad (44b)$$

Otherwise, (38) must be integrated numerically.

To evaluate accuracy of approximate analytical results (43) and (44), ℓ_{T1} and ℓ_{T2} are plotted vs depth in figures 2, 3, and 4 and compared to $\ell_T(z; z_o, \ell_o)$, obtained by numerically integrating (38) with $v = v_-$ given by (42). For the sake of example, $f = 1$ and $RTGK/4\pi = 10^6$ meters/sec (Wyman, et al 1952) are used in all three models, and $\ell_{T1}(z)$, $\ell_{T2}(z)$ and $\ell_T(z)$ are represented for various initial radii, ℓ_o , at $z_o = -20$ meters. Note that ℓ_{T1} is a good approximation to ℓ_T for $30\mu < \ell < 100\mu$ (viscous regime) and that ℓ_{T2} closely approximates ℓ_T for $\ell > 400\mu$ (turbulent regime). Neither (43) nor (44) is valid for $\ell \approx 30\mu$ because they neglect surface tension, and neither is accurate in the transition region $100\mu < \ell < 400\mu$.

An example of the phenomenon analyzed by LeBlond is evident in Figures 2-4. As a bubble rises under buoyancy it tends to expand as the hydrostatic pressure decreases, but it also tends to contract as gas diffuses across the bubble's surface. If a bubble's radius is less than some critical radius, ℓ_b , it rises too slowly, shrinks monotonically, and disappears before reaching the surface because gas diffusion dominates hydrostatic expansion. If its radius is greater than another critical radius, ℓ_a , it will expand monotonically as it rises because hydrostatic expansion dominates gas diffusion. For an initial radius between ℓ_a and ℓ_b , the bubble's behavior is not necessarily monotonic; it may or may not reach the surface.

Bubbles with radii less than ℓ_b will rise a finite distance before disappearing, and computed values of ℓ_a and ℓ_b depend upon the gas diffusion model used as well as parameters like z_o . Examination of ℓ_T in Figures 2-4

indicates that $\ell_a \sim 400\mu$ and $\ell_b \sim 250\mu$, while a 100μ bubble rises about 1.1 meters. Unfortunately there is usually insufficient information available for an accurate specification of the gas diffusion phenomenon. For example, in (29) the gas diffusion rate depends not only upon the partial pressure $f(z)$, but also upon the parameters G and K which are determined by the type of gas and the presence of surface active materials. This data is often unavailable for the ocean. Since characteristic curves and bubble distributions (ref. Figures 5-12) are sensitive to the gas diffusion rate, specification of the unknown parameters is important, and it may require a sequence of educated guesses refined from comparisons of computed and observed distributions.

If the fluid velocity \vec{V} is not negligible and the problem is multi-dimensional, the computation of characteristic curves is more difficult. In general, equations for x, y, v_x, v_y , and v_z must be integrated simultaneously with (38). However, if $d\vec{V}/dt$ given by (18) is small compared to the other terms in (17), a useful approximation (that eliminates the three characteristic equations for velocity) might be

$$\vec{V} \approx \vec{V} + v_T \hat{k},$$

where v_T is the terminal velocity of the rising bubble.

2. Bubble Distribution

Since bubbles rise in a quiescent fluid at very nearly their terminal velocity,

$$\phi(z, v, \ell) = \delta(v - v_T) \phi(z, \ell) \quad (45)$$

should be a good approximation where v_T is given either empirically or by (39), (40) or (42). In this equation

$$\Phi(z, \ell) \equiv \int_{-\infty}^{\infty} \phi(z, v, \ell) dv \quad (46)$$

is the 'radius density,' the number of bubbles per unit volume per unit radius.

Equation (35) can be integrated over v to yield

$$\Phi(z, \ell) = (v_{T0}/v_T) \Phi(z_0, \ell_0) (\partial \ell_0 / \partial \ell) + (1/v_T) \int_{z_0}^z s(z', \ell') (\partial \ell' / \partial \ell) dz' \quad (47)$$

with

$$s(z', \ell') \equiv \int_{-\infty}^{\infty} S(z', v', \ell') dv', \quad (48)$$

where $d\ell_0 = (\partial \ell_0 / \partial \ell) d\ell$ and $d\ell' = (\partial \ell' / \partial \ell) d\ell$ have been used. The bubble density,

$$\Phi(z) \equiv \int_0^{\infty} \Phi(z, \ell) d\ell, \quad (49)$$

which is the total number of bubbles per unit volume at depth z , regardless of radius, is given by (47) integrated over all radii,

$$\Phi(z) = \int_0^{\infty} (v_{T0}/v_T) \Phi(z_0, \ell_0) d\ell_0 + \int_0^{\infty} \int_{z_0}^z (1/v_T) s(z', \ell') (\partial \ell' / \partial \ell_0) dz' d\ell_0. \quad (50)$$

It must be remembered that v_T and v_{T0} , as well as ℓ and ℓ' , are functions of ℓ_0 and that integrations in z are taken along the characteristic curves

$$\{z', v_T(z'; z_0, \ell_0), \ell_T(z'; z_0, \ell_0) : z_0 \leq z' \leq z\}, \quad (51)$$

where ℓ_T is obtained by integrating (38) with $v = v_T$.

For most applications the radius density provides adequate information. To calculate this function for a given z and ℓ , one needs $\partial \ell' / \partial \ell$, ℓ' , and $s(z', \ell')$ at points on the characteristic curve that passes through (z, ℓ) so the integral in (47) can be evaluated. Using notation from the appendix,

$$\partial \ell' / \partial \ell = 1 / \gamma_{77}(z, z'), \quad (52)$$

where γ_{77} satisfies the differential equation obtained by setting $v = v_T$ in (38) and taking the partial derivative with respect to ℓ' :

$$d\gamma_{77}/dz = F_{77} \gamma_{77} \quad (53)$$

with the boundary condition

$$\gamma_{77}(z, z) = 1$$

where

$$F_{77}(z; z_0, \ell_0) = \{ (2\Gamma/\ell^2) [\ell - (3\delta RT/v_T) (D(1-f) - z + \Gamma/\ell)] [3(D-z) + 2\Gamma/\ell]^{-1} + [1 + (3\delta RT/v_T) [\Gamma/\ell^2 + (D(1-f) - z + \Gamma/\ell) (\partial v_T / \partial \ell) / v_{T1}]] [3(D-z) + 2\Gamma/\ell]^{-1} \} \quad (54)$$

in which $(GK/4\pi) = \text{constant} \equiv \delta$ (Wyman, et al, 1952) has been used. When the approximation $v_T = v_-$ (42) is used,

$$\partial v_T / \partial \ell = (3v_{T1}/\ell) [1 + 4Q^2]^{-1/2} - v_-/\ell. \quad (55)$$

The solution to (53) is

$$\gamma_{77}(z, z') = \exp[\mathcal{F}(z, z')] \quad (56)$$

with

$$\mathcal{F}(z, z') \equiv \int_{z'}^z F_{77}(z''; z_0, \ell_0) dz'',$$

and it is obvious that

$$\gamma_{77}(z, z') = \gamma_{77}(z, z_0) / \gamma_{77}(z', z_0). \quad (57)$$

Using (56) and (57), (47) can be written

$$\begin{aligned} \phi(z, \ell) = & [\exp[-\mathcal{F}(z, z_0)] / v_T] \{ v_{T0} \phi(z_0, \ell_0) + \\ & + \int_{z_0}^z s(z', \ell') \exp[\mathcal{F}(z', z_0)] dz' \} \end{aligned} \quad (58)$$

Once the source $s(z, \ell)$ has been specified, (56) can be used to evaluate the radius density at points along any characteristic curve (51) obtained by integrating (33). In the following discussion of sample calculations, $\phi(z, \ell)$ will refer to the radius density when the approximation $v_T = v_-$ (42) is used.

If either approximation (43) or (44) is appropriate, then either

$$\partial \ell' / \partial \ell = [(D-z)/(D-z')] [\ell^2 / \ell'^2] \quad (43c)$$

or

$$\partial \ell' / \partial \ell = [(D-z)/(D-z')]^{1/2} [\ell / \ell']^{1/2}, \quad (44c)$$

is used in (47) to obtain the approximate radius density $\phi_1(z, \ell)$ or $\phi_2(z, \ell)$, respectively, at points along the characteristic curve (51) with $\ell_T = \ell_{T1}$, or $\ell_T = \ell_{T2}$, respectively. If gas diffusion can also be neglected ($GK = 0$) then both approximations reduce to

$$\ell = \ell_{T3}(z; z_0, \ell_0) = [(D-z_0)/(D-z)]^{1/3} \ell_0 \quad (59)$$

which can be used in (47) and (51) to obtain the approximate radius density $\phi_3(z, \ell)$.

3. Numerical Results

For the sake of example, consider the situation investigated by McCartney and Bary (1965) who acoustically measured rather large gas bubbles ascending from the bottom of Saanich Inlet, B. C., and inferred the bottom source represented in Figure 5 from the ascent velocities. If we model that ocean as 1-D and quiescent, then equation (47) can be used to infer the radius density throughout the volume. Since volume sources produce mainly smaller bubbles that their measurements do not include, only the plane source $\bar{\phi}(z_0, \ell_0)$ (Figure 5) at $z_0 = -197$ meters is considered in this sample calculation, and (47) reduces to

$$\bar{\phi}(z, \ell) = (v_{T0}/v_T) \bar{\phi}(z_0, \ell_0) (\partial \ell_0 / \partial \ell). \quad (60)$$

Using $f = 1$, approximations $\bar{\phi}$, $\bar{\phi}_1$, $\bar{\phi}_2$, and $\bar{\phi}_3$ to the radius were computed at various depths between $z = -197\text{m}$ and $z = 0$. $\bar{\phi}(z, \ell)$ (solid line) and $\bar{\phi}_3(z, \ell)$ (dashed line) are plotted in Figures 6-10 at the depths $z = -172\text{m}, -147\text{m}, -122\text{m}, -97\text{m}, -47\text{m}$, and 0m . Although actual calculations do not yield precisely rectangular distributions for $z \neq z_0$, $\bar{\phi}$ and $\bar{\phi}_3$ and drawn as perfect histograms because the error introduced is negligible.

While $\bar{\phi}_3$ neglects gas diffusion and surface tension, $\bar{\phi}$ includes these effects. For the gas diffusion model used, all bubble radii for which $\bar{\phi}(z_0, \ell_0)$ is nonzero lie below the critical radius ℓ_b , so these bubbles will shrink monotonically as they rise and will disappear before reaching the surface. The distribution $\bar{\phi}$ is seen to shift toward smaller radii as depth decreases, until even the largest bubbles have disappeared by the time $z \sim -90\text{m}$, so only $\bar{\phi}_3$ is shown in Figure 10. Since $\ell_b = 0$ in the model used to calculate $\bar{\phi}_3$, these bubbles necessarily expand as they rise, and the distribution shifts monotonically to larger radii.

The bubble density is simply the area under the histogram. As z increases from -197m the density of $\phi(z, l)$ initially increases since flux is conserved and the bubbles are slowing down and piling up. However, nearer the surface, most smaller bubbles have succumbed to gas diffusion and the density starts to decrease toward zero. For $\phi_3(z, l)$ the density is seen to decrease as z increases since the bubbles are accelerating and becoming spread out.

The distributions ϕ_2 and ϕ_3 are not shown because neither follows ϕ closely. ϕ_2 is the best approximation, but these bubbles do not quite shrink fast enough. Some of the bubbles in ϕ_1 contract monotonically while others contract and then expand. For the model used most of the bubbles originate at the bottom with radii in the transition region, $l_a < l_o < l_b$, where neither approximations (43) nor (44) are valid.

Interestingly enough, the experimental results of McCartney and Bary (1965) indicate the bubbles from the bottom of Saanich Inlet expand as they rise according to the distribution ϕ_3 , which ignores gas diffusion. Thus, it appears that diffusion is somehow inhibited across the surfaces of these bubbles which are composed of "gas released from the highly organic, anaerobic sediment of the bottom," possibly methane. Either the water was saturated with respect to the gas(es) in the bubbles, or these bubbles were coated with an active material that severely impeded gas diffusion. While it is significant to note that ϕ is calculated using $GK/4\pi = \delta$ (eqn. (30)), which is based upon experiments with relatively clean air bubbles (Wyman, et al 1952), and that $f = 1$ at all depths is not physically realistic, certain qualitative conclusions, based on a comparison of ϕ and ϕ_3 to the observed distribution, are still valid. For example, gas diffusion appears to be negligible in this situation; and gas diffusion would profoundly affect the bubble distribution. The latter observation emphasizes the fact that results are strongly dependent on the bubble dynamics and ocean models used.

As the basis for a second sample calculation, consider the supposition that the observed bubble distribution indicates the functional dependence of the volume source. To test this idea, consider a hypothetical volume source suggested by the measurements of Shulkin (1968) and Medwin (1970):

$$s(z, \ell) = e^{z/h} L(\ell) \quad (61)$$

where

$$L(\ell) = \begin{cases} (\ell/\ell')^{-3.5} & \text{for } \ell \geq \ell' \\ 0, & \text{for } 0 \leq \ell < \ell' \end{cases} \quad (62)$$

with $h = 10$ meters and $\ell' = 20\mu$. Physically, a source decaying exponentially with depth might arise from photosynthesis, light sensitive bacteria, wave action, etc. Medwin (1970) has observed an exponential behavior for small bubbles ($\ell < 60\mu$), and both Medwin (1970) and Shulkin have observed that the near surface bubble density appears to fall off like some power of the bubble radius. The radius spectrum $L(\ell) \sim \ell^{-3.5}$ is chosen as an example.

Assuming that the source is zero below $z = -30$ meters, and that $f = 1$, the radius density was computed using $v_T = v_{\infty}$ in (38) and (58). Figures 11 & 12 presents log-log plots of $\Phi(z, \ell)$ (solid line) and $s(z, \ell)$ (dashed line) vs radius for four depths, $z = -29\text{m}$, -20m , -10m , and 0m . A comparison of Φ and s indicates that the distribution follows approximately the functional form of the source for $\ell > 100\mu$:

$$\Phi(z, \ell) \sim e^{z/h'} \ell^{-3.5} \quad (63)$$

$h' = 6.5\text{m}$. The distribution at $z = -29$ meters does not fit this pattern because it is too near the region assumed to be devoid of bubbles.

For $\ell < 100\mu$ the functional form of Φ is more complicated and does not necessarily follow (63). Except at the surface, the curves are all concave down which indicates a deficiency of small bubbles. Gas diffusion and surface

tension cause small bubbles to disappear much more rapidly than large bubbles. While the small bubbles observed at a given depth originate primarily from local sources, many of the larger bubbles observed originate at sources distributed well below that depth. However, for the model used, gas diffusion decreases rapidly with depth, so there is less discrimination against the small bubbles in the near surface region. From Figures 11 and 12,

$$\bar{\phi}(0, \ell) \sim \ell^{-3.75} \quad (64)$$

These results indicate that if gas diffusion is significant, the small bubble sources will probably fall off to a higher power in ℓ than the observed distribution, but the larger bubble sources may have roughly the same ℓ -dependence as the observed distribution. Furthermore, the depth dependence of the bubble sources is likely to be functionally similar to that of the bubble population. Of course these qualitative relationships between bubble population and bubble source are not likely to be applicable unless the model is valid. For example, any of the following can have a profound influence on the bubble distribution and its relationship to the source: A significant fluid velocity, $\vec{V} \neq 0$, a partial pressure, $f(z)$, that varies with depth, or surface active materials that impede gas diffusion (e.g., lower K in equation (24)).

The distributions $\bar{\phi}_1$ and $\bar{\phi}_2$ were also computed for this example but are not displayed. As expected, $\bar{\phi}_1$ approximates $\bar{\phi}$ fairly well for $30\mu < \ell < 100\mu$, and $\bar{\phi}_2$ is a good approximation to $\bar{\phi}$ for $\ell > 350\mu$.

VI. CONCLUSIONS

The main purpose of this paper has been to develop the general framework of bubble transport theory and then to demonstrate its application. The bubble transport equation and its solution relate the ensemble average behavior of a bubble population to dynamics of a single bubble and to properties of the transporting fluid. Among the most important aspects of gas bubble dynamics in liquids are bubble gas diffusion and drag, which depend upon many different physical parameters. For the upper ocean, information concerning these parameters, as well as information about bubble sources and fluid velocity fields, is usually incomplete. In this case, bubble transport theory cannot be used to predict bubble distributions; its primary utility is as an analytical tool for investigating relationships among the various complex factors that affect the distribution and for refining models of the upper ocean. Future work will be concerned with analysis of more complex ocean models.

APPENDIX

It is shown here that the Jacobian,

$$\gamma(t, t') = \frac{\partial(\vec{r}, \vec{v}, \ell)}{\partial(\vec{r}', \vec{v}', \ell')} \quad , \quad (\text{A-1})$$

used to transform the volume element $d^7\tau$ between two points on a characteristic curve,

$$d^3r d^3v d\ell = \gamma(t, t') d^3r' d^3v' d\ell' \quad , \quad (\text{A-2})$$

satisfies the differential equation

$$d\gamma/dt = \Sigma_t \gamma \quad . \quad (\text{A-3})$$

Using the boundary condition $\gamma(t, t') = 1$, this equation can be integrated to obtain

$$\gamma(t, t') = \exp \left[\int_{t'}^t \Sigma_t(t''; \vec{r}_0, \vec{v}_0, \ell_0) dt'' \right] \quad (\text{A-4})$$

where the indicated integration is along the characteristic curve passing through $(\vec{r}', \vec{v}', \ell')$ and (\vec{r}, \vec{v}, ℓ) .

Referring to the notation (5), define the elements of a 7 x 7 matrix

$$\gamma_{ij} = \partial q_i / \partial q_j' \quad , \quad i, j = 1, 2, \dots, 7 \quad (\text{A-5})$$

then the Jacobian is the determinant of this matrix,

$$\gamma = \det((\gamma_{ij})) = \sum_{\substack{i \\ (\text{or } j)}} (-1)^{i+j} \gamma_{ij} C_{ij} \quad , \quad (\text{A-6})$$

where C_{ij} is the "minor" of the element γ_{ij} (C_{ij} is γ with the i^{th} row and j^{th} column deleted).

If the following elements are defined,

$$R_1 \equiv v_x, R_2 \equiv v_y, R_3 \equiv v_z, R_4 \equiv a_x \quad (A-7)$$

$$R_5 \equiv a_y, R_6 \equiv a_z, \text{ and } R_7 \equiv v$$

then the characteristic equations (11) can be written

$$dq_i/dt = R_i(q_1, q_2, \dots, q_7, t) \quad i = 1, 2, \dots, 7 \quad (A-8)$$

Taking the partial derivatives of these equations with respect to the q_j ' and using the chain rule, the set of differential equations for the γ_{ij} is obtained:

$$\frac{d\gamma_{ij}}{dt} = \frac{\partial R_i}{\partial q_j} = \sum_k \frac{\partial R_i}{\partial q_k} \gamma_{kj}, \quad i, j, = 1, 2, \dots, 7 \quad (A-9)$$

These equations are used to expand the derivative of (A-6) taken with respect to the parameter t :

$$\frac{d\gamma}{dt} = \sum_i \sum_j (-1)^{i+j} \frac{d\gamma_{ij}}{dt} C_{ij} = \sum_{i,j} (-1)^{i+j} C_{ij} \sum_k \frac{\partial R_i}{\partial q_k} \gamma_{kj} \quad (A-10)$$

Using (A-6), this expression can be rearranged to yield the following:

$$\begin{aligned} \frac{d\gamma}{dt} &= \sum_{i,j} (-1)^{i+j} C_{ij} \left\{ \frac{\partial R_i}{\partial q_i} \gamma_{ij} + \sum_{k \neq i} \frac{\partial R_i}{\partial q_k} \gamma_{kj} \right\} \\ &= \gamma \sum_i \frac{\partial R_i}{\partial q_i} + \sum_{i, k \neq i} (-1)^i \frac{\partial R_i}{\partial q_k} \sum_j (-1)^j \gamma_{kj} C_{ij} \end{aligned} \quad (A-11)$$

The term $\sum_i (-1)^j \gamma_{kj} C_{ij}$ is zero since $k \neq i$. This can most easily be seen by expanding each determinant C_{ij} by minors of the elements γ_{km} , $m \neq j$.

Since

$$\sum_i \frac{\partial R_i}{\partial q_i} = \vec{v}_v \cdot \vec{a} + \frac{\partial v}{\partial \ell} \equiv \sum_t \quad (\text{A-12})$$

the result (A-2) is obtained.

REFERENCES

1. Blanchard, D. C. and Woodcock, A. H. 1957 Tellus 9, 145.
2. Case, K. M. and Zweifel, P. F. 1967 Linear Transport Theory, Addison-Wesley.
3. Ceschino, F. and Kuntzman, J. 1966 Numerical Solution of Initial Value Problems, Prentice-Hall.
4. Chapman, S. and Cowling, T. G. 1964 The Mathematical Theory of Nonuniform Gases, Cambridge University Press.
5. Datta, R. L., Napier, D. H. and Newitt, D. M. 1950 Trans. Inst. Chem. Engrs., Lond. 23, 14.
6. Fox, F. E. and Herzfeld, K. F. 1954 J. Acous. Soc. 26, 984.
7. Garabedian, P. R. 1964 Partial Differential Equations, Wiley.
8. Glotov, V. P., Kolobaev, P. A., and Neuimin, G. G. 1962 Sov. Phys.-Acous. 7, 341.
9. Karwisher, J. 1963 Deep-Sea Res. 10, 195.
10. LeBlond, P. H. 1969 J. Fluid Mech. 35, 711.
11. LeBlond, P. H. 1969 J. Fluid Mech. 38, 861.
12. Levich, V. G. 1962 Physicochemical Hydrodynamics, Prentice-Hall.
13. McCartney, B. S. and Bary, B. Mck. 1965 Deep-Sea Res. 12, 285.
14. Medwin, H. 1970 J. Geophys. Res. 75, 599.
15. Monahan, E. C. and Zietlow, C. R. 1969 J. Geophys. Res. 74, 6961.
16. Shonting, D. H. 1968 J. Marine Res. 26, 43.
17. Shulkin, M. 1968 J. Acous. Soc. Amer. 44, 1152.
18. Shulkin, M. 1969 J. Acous. Soc. Amer. 45, 1054.
19. Sutcliffe, W. H., Jr., Baylor, E. R. and Menzel, D. W. 1963 Deep-Sea Res. 10, 233.
20. Wyman, J., Jr., Scholander, P. F., Edwards, G. A. and Irving, L. 1952 J. Marine Res. 11, 47.

LIST OF FIGURE CAPTIONS

Figure 1:

The velocity, v , of bubbles starting at rest and rising from an initial depth $z_0 = -20$ meters. The initial radius is ℓ_0 , (in microns), the terminal velocity is v_T , and $(z-z_0)$ is the height above the release point.

Figures 2, 3, and 4:

Bubble radius in microns as a function of depth in meters for various initial radii, ℓ_0 (at $z_0 = -20$ meters), calculated using three different expressions for the terminal velocity, v_T . The solid line is ℓ_{T1} , obtained by integrating (38) with $v = v_-$ (equation 42), the broken line is ℓ_{T1} (equation 43a), and the dashed line is ℓ_{T2} (equation 44a). The gas diffusion model used (Wyman, et al 1952) assumes a uniform partial pressure of one atmosphere, $f = 1$, and $RTGK/4\pi = 10^{-6}$ meters/second.

Figure 5 :

The distribution, $\phi(z_0, \ell_0)$, in relative units, of bubbles rising off the bottom of Saanich Inlet, B. C. (McCartney and Bary 1965) where $z_0 = -197$ meters and the bubble radius, ℓ_0 , is in microns.

Figures 6, 7, 8, and 9:

The distributions $\phi(z, \ell)$ (solid line) and $\phi_3(z, \ell)$ (dashed line) in relative units at the depths $-172m$, $-147m$, $-122m$, and $-97m$ where bubble radius, ℓ , is in microns. ϕ_3 neglects gas diffusion while ϕ assumes a uniform partial pressure of one atmosphere, $f = 1$, and $RTGK/4\pi = 10^{-6}$ meters/sec (Wyman, et al 1952).

Figure 10:

The distribution, $\phi_3(z, \ell)$, in relative units, vs radius, ℓ , in microns, for $z = -47m$ and $z = 0$.

Figures 11 and 12:

The distribution, $\phi(z, \ell)$ (solid lines), in relative units, vs radius, ℓ , in microns, for various depths, in meters, from a distributed source, $s(z, \ell)$ (dashed lines; equations 61 and 62). The same gas diffusion model used to calculate ϕ in Figure 5 is used in this example.

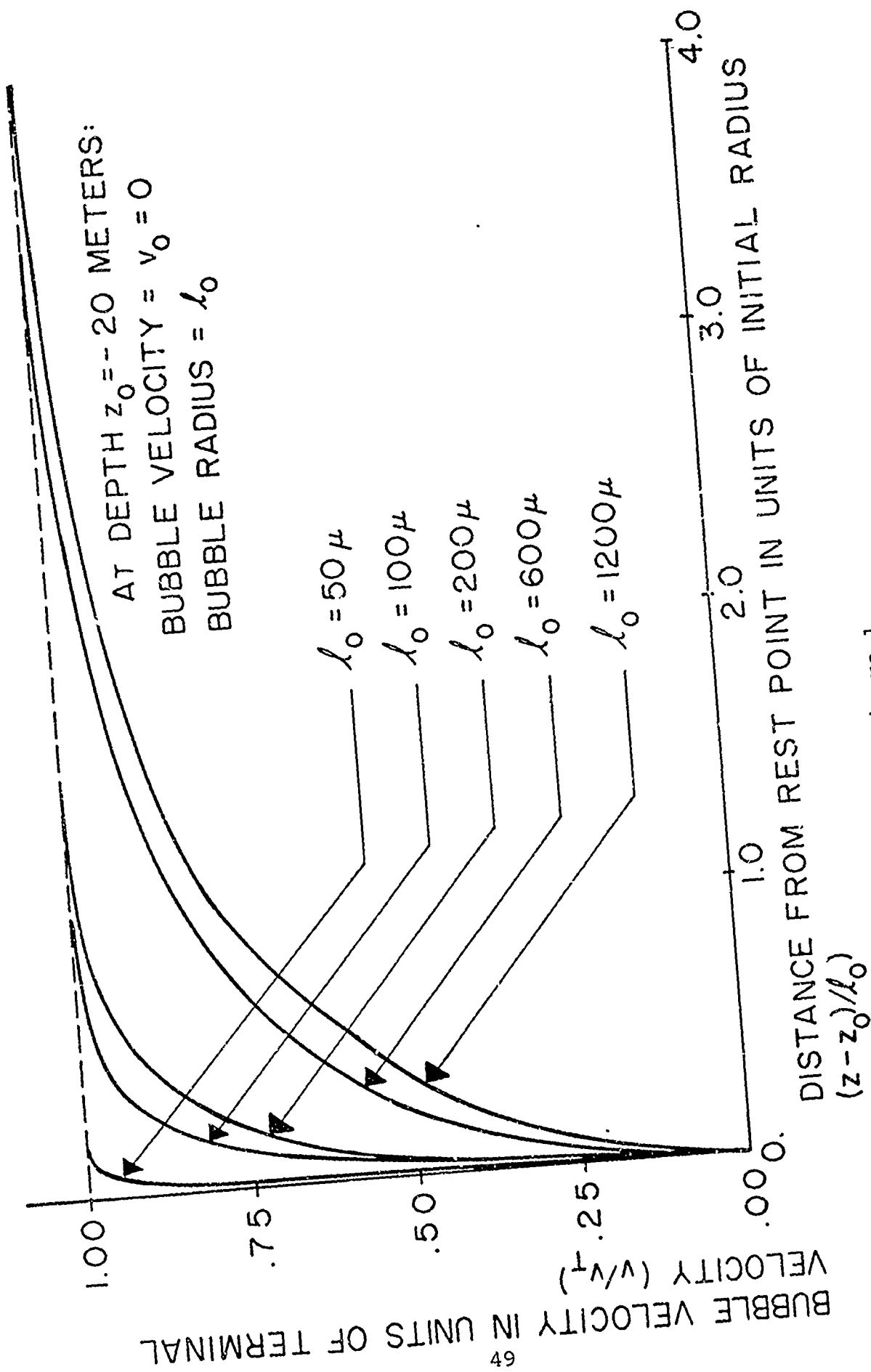


Figure 1

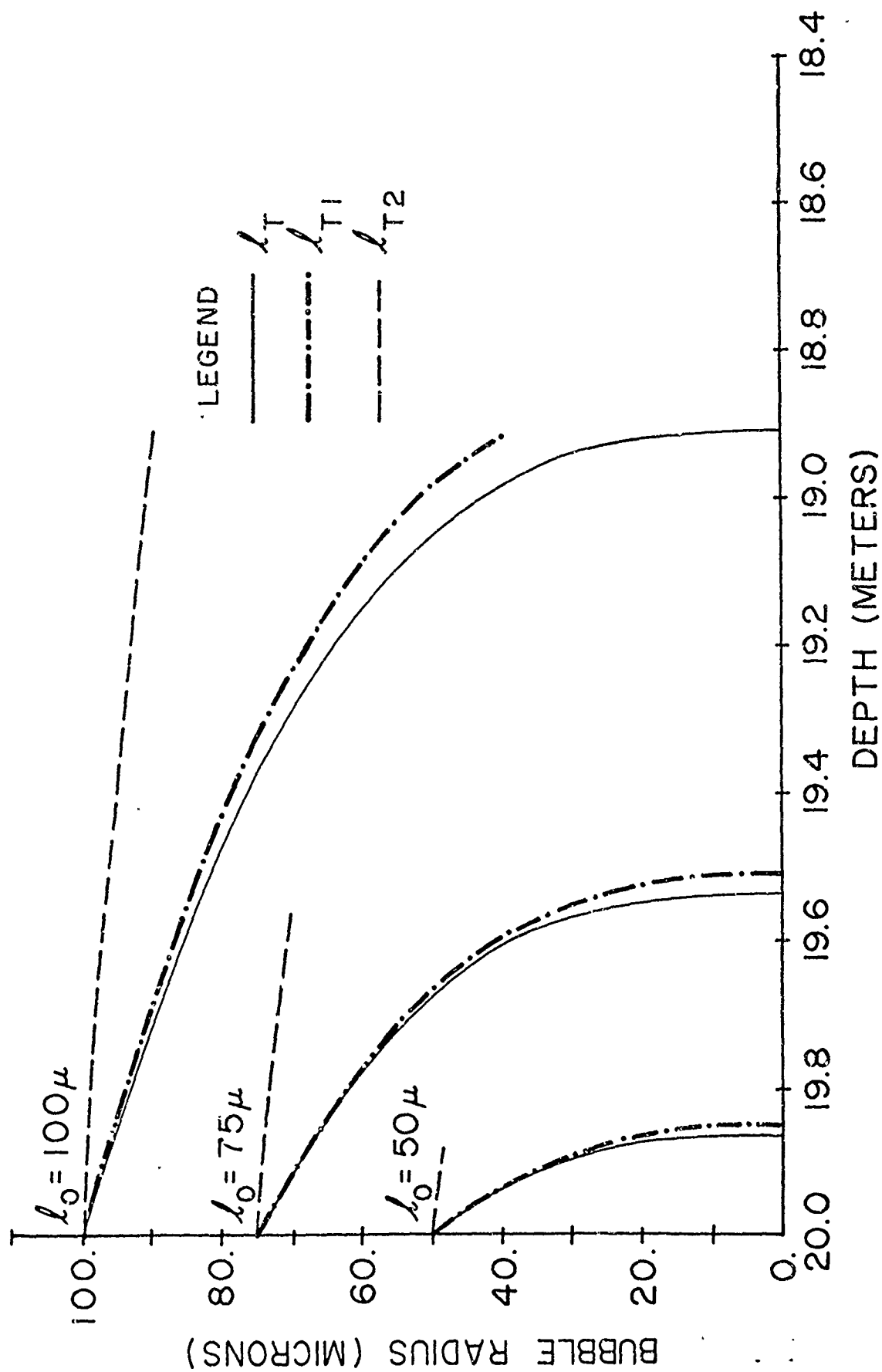


Figure 2

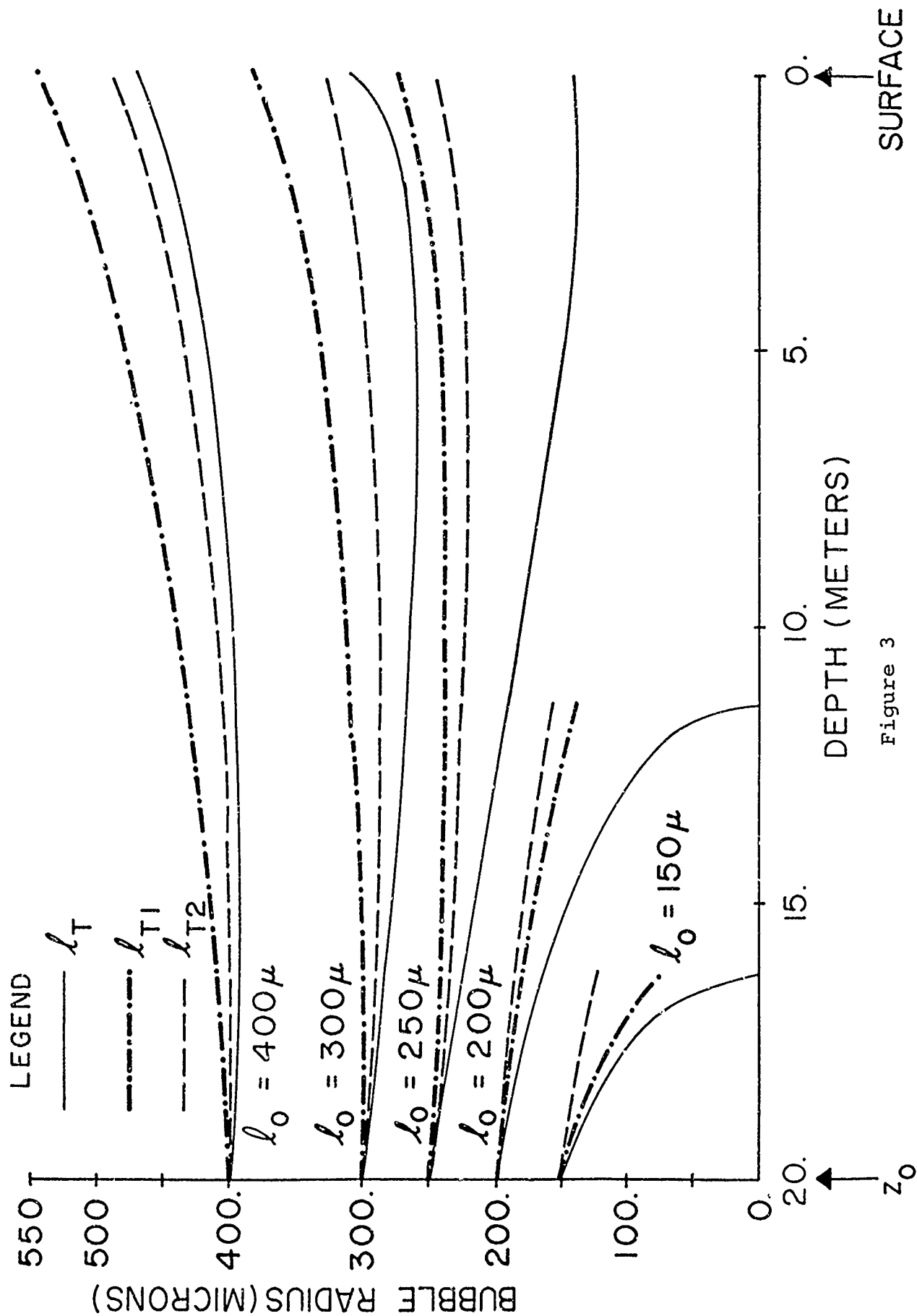


Figure 3

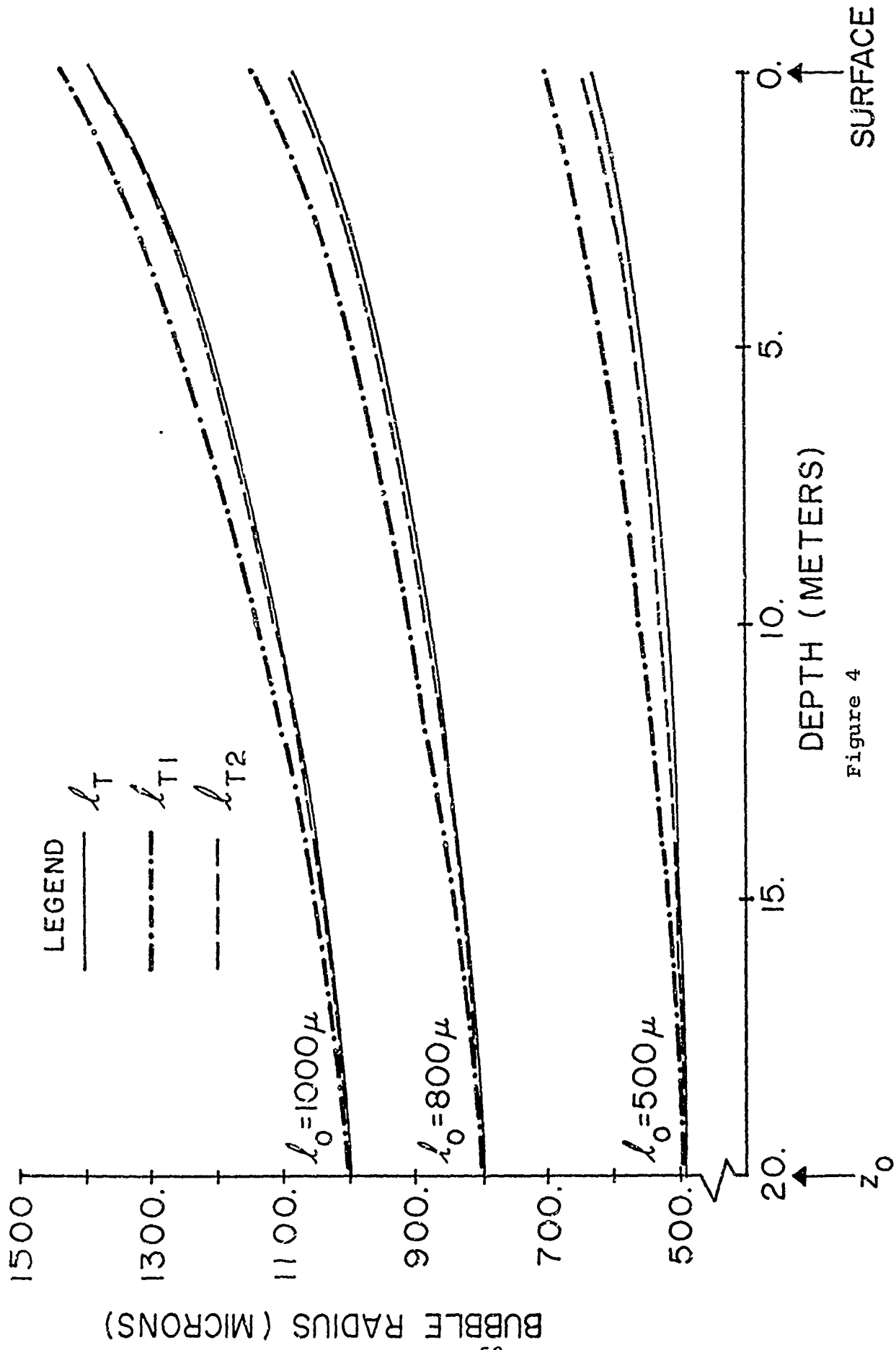


Figure 4

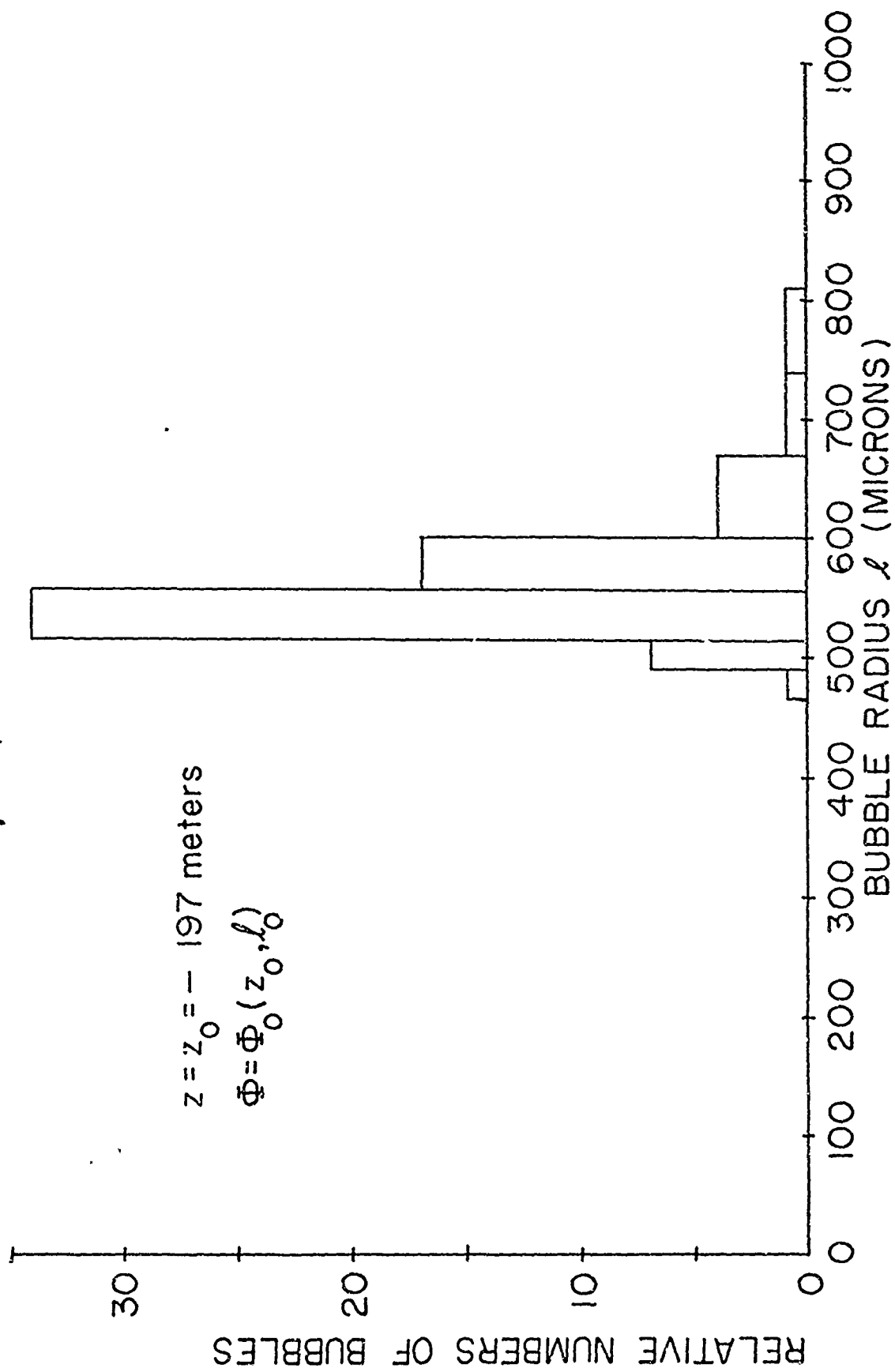


Figure 5

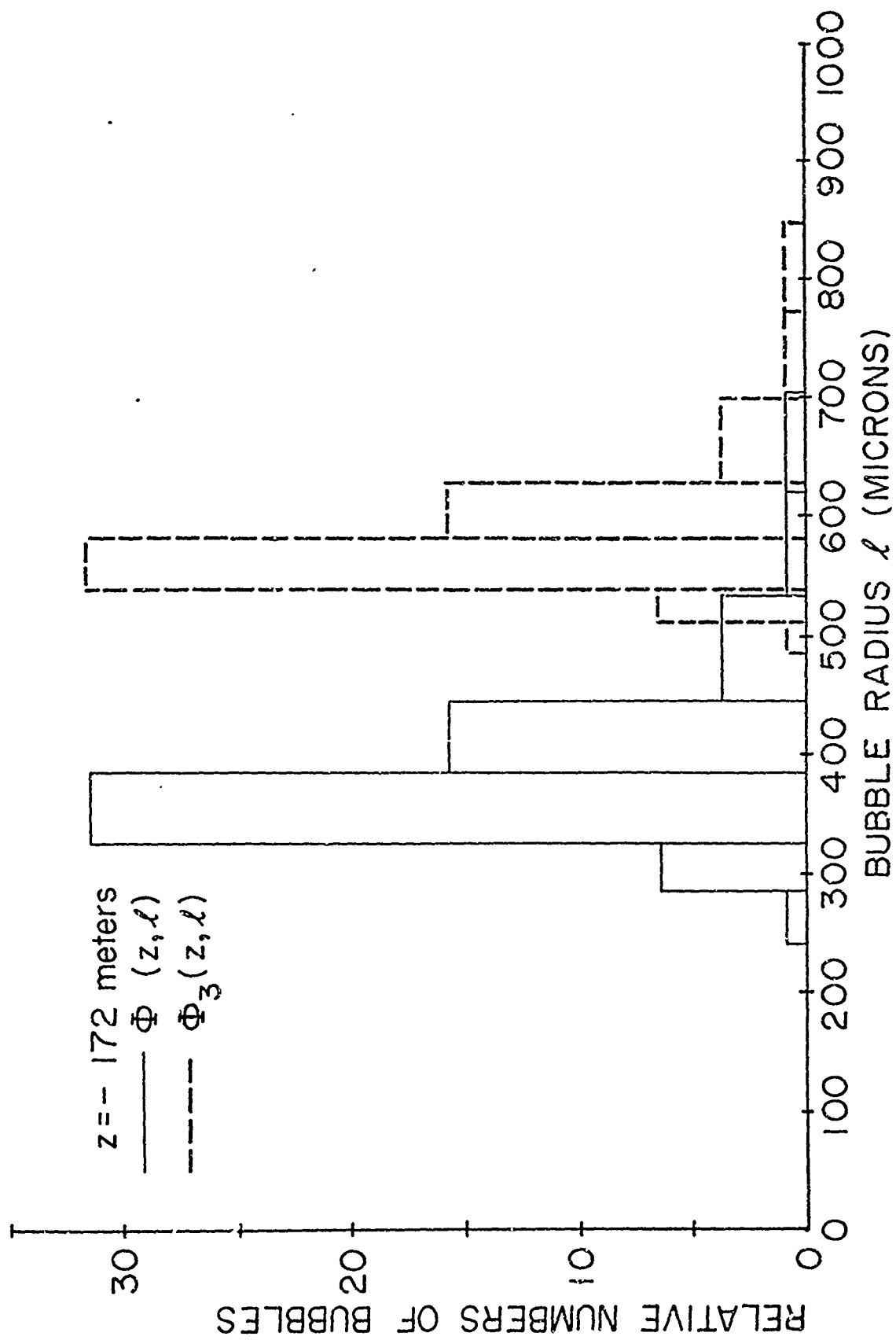


Figure 6

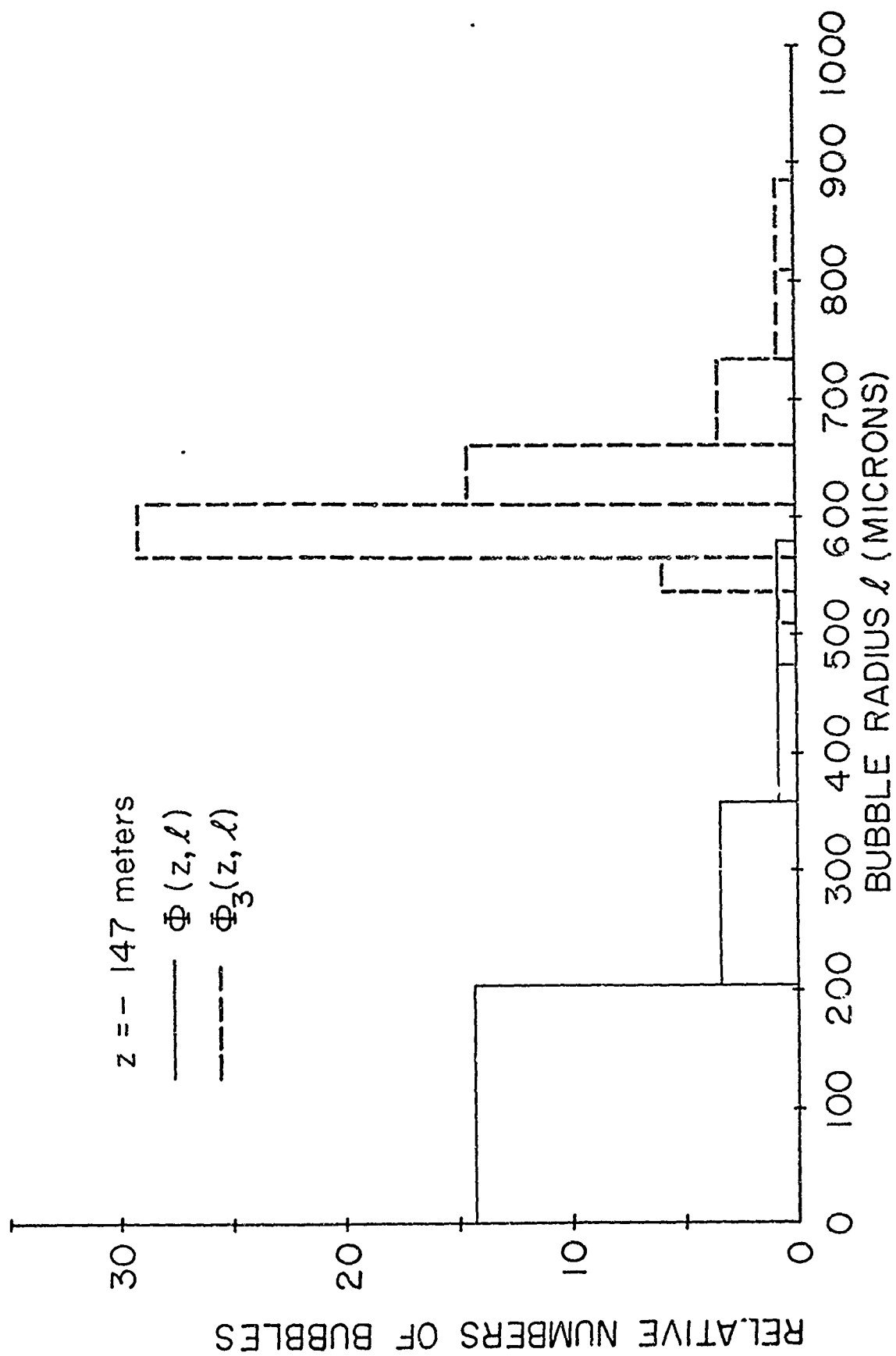


Figure 7

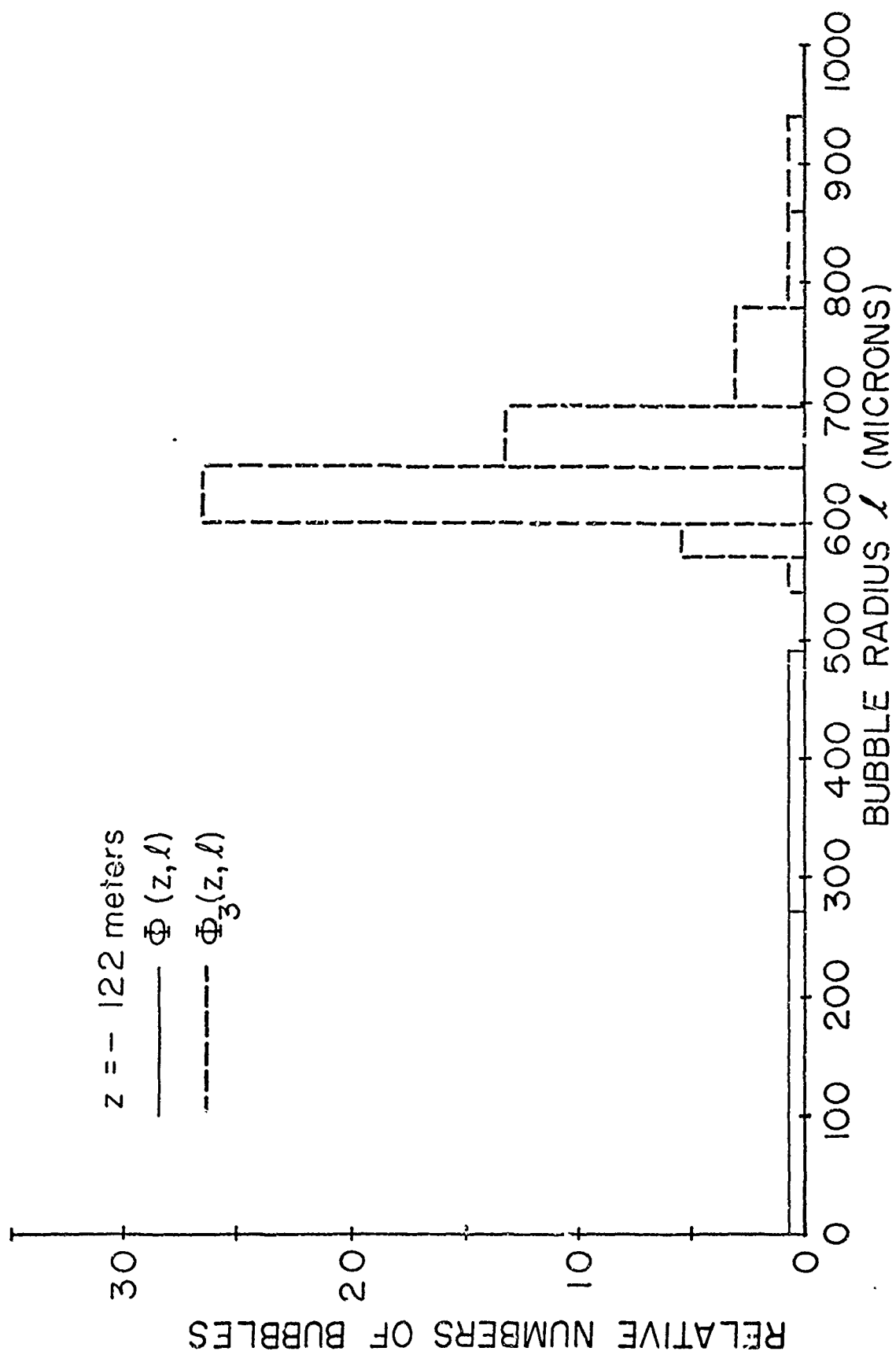


Figure 8

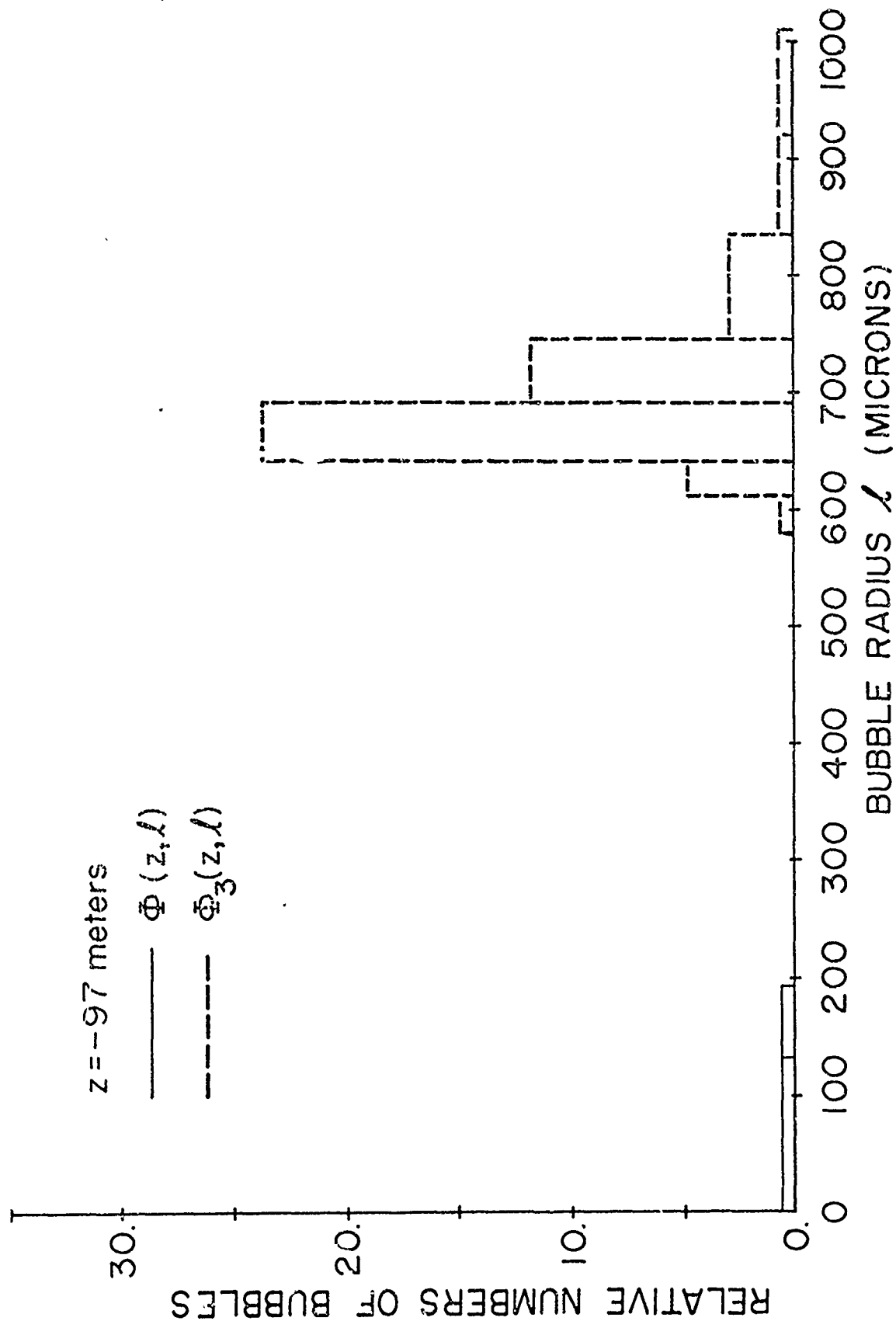


Figure 9

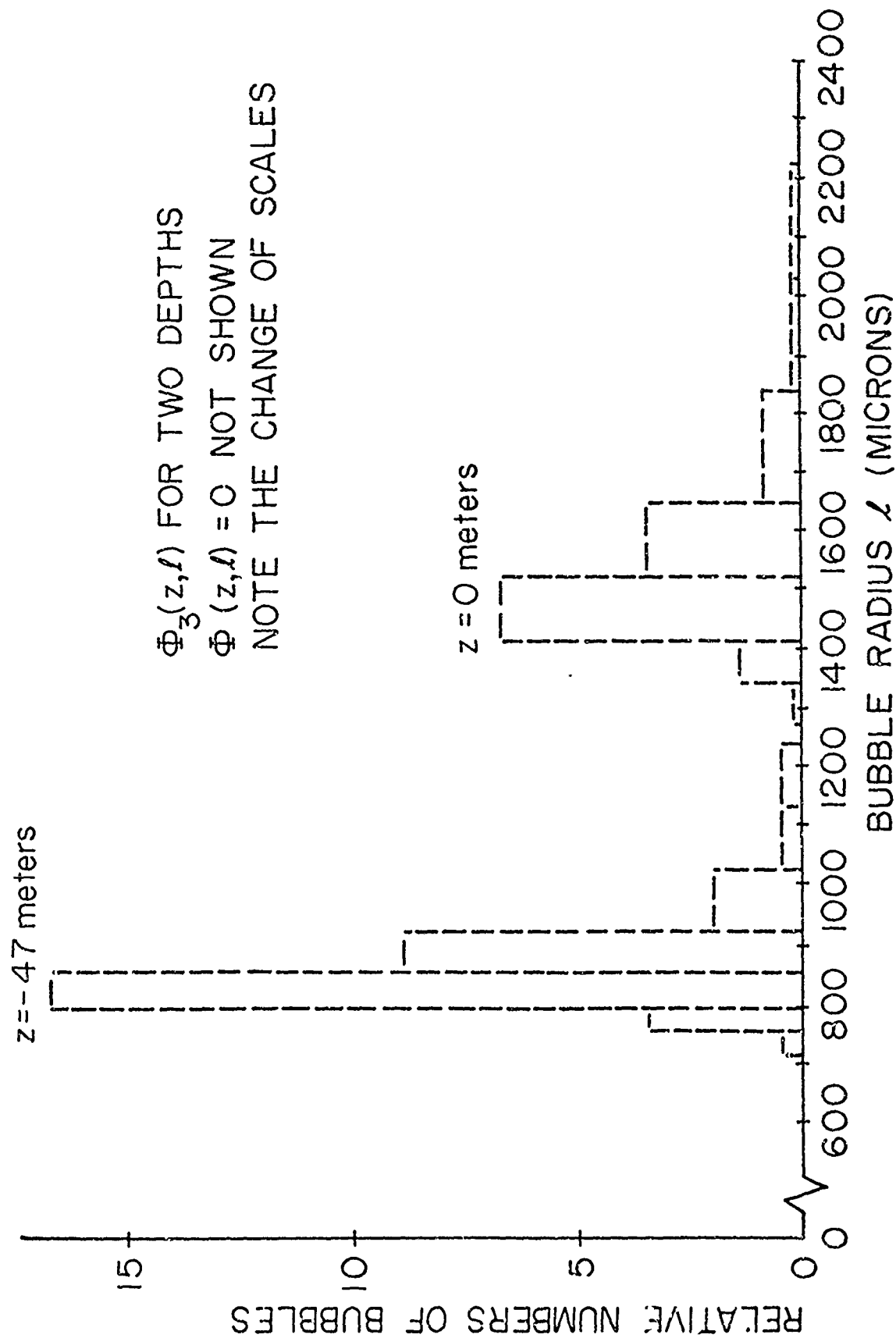


Figure 10

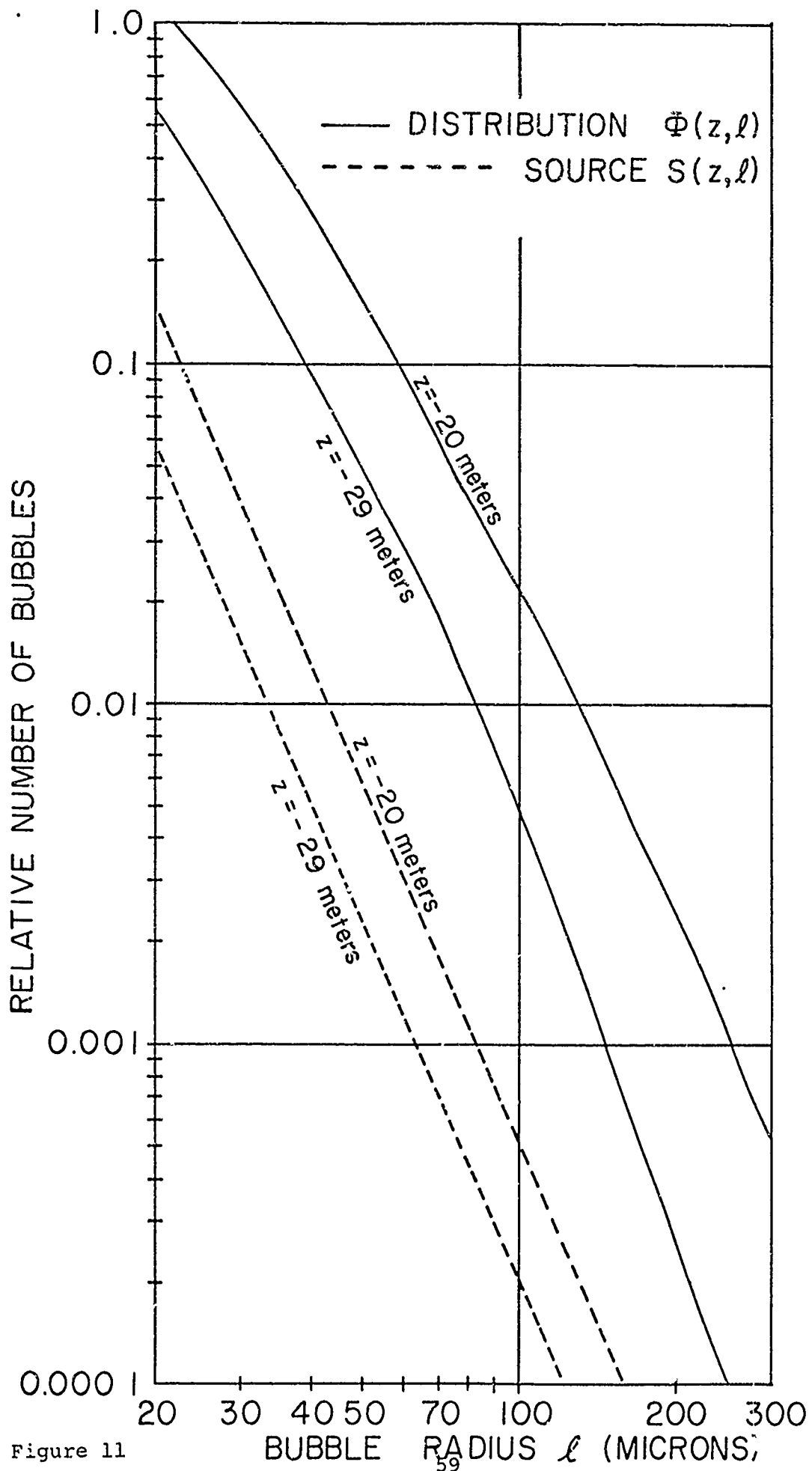


Figure 11

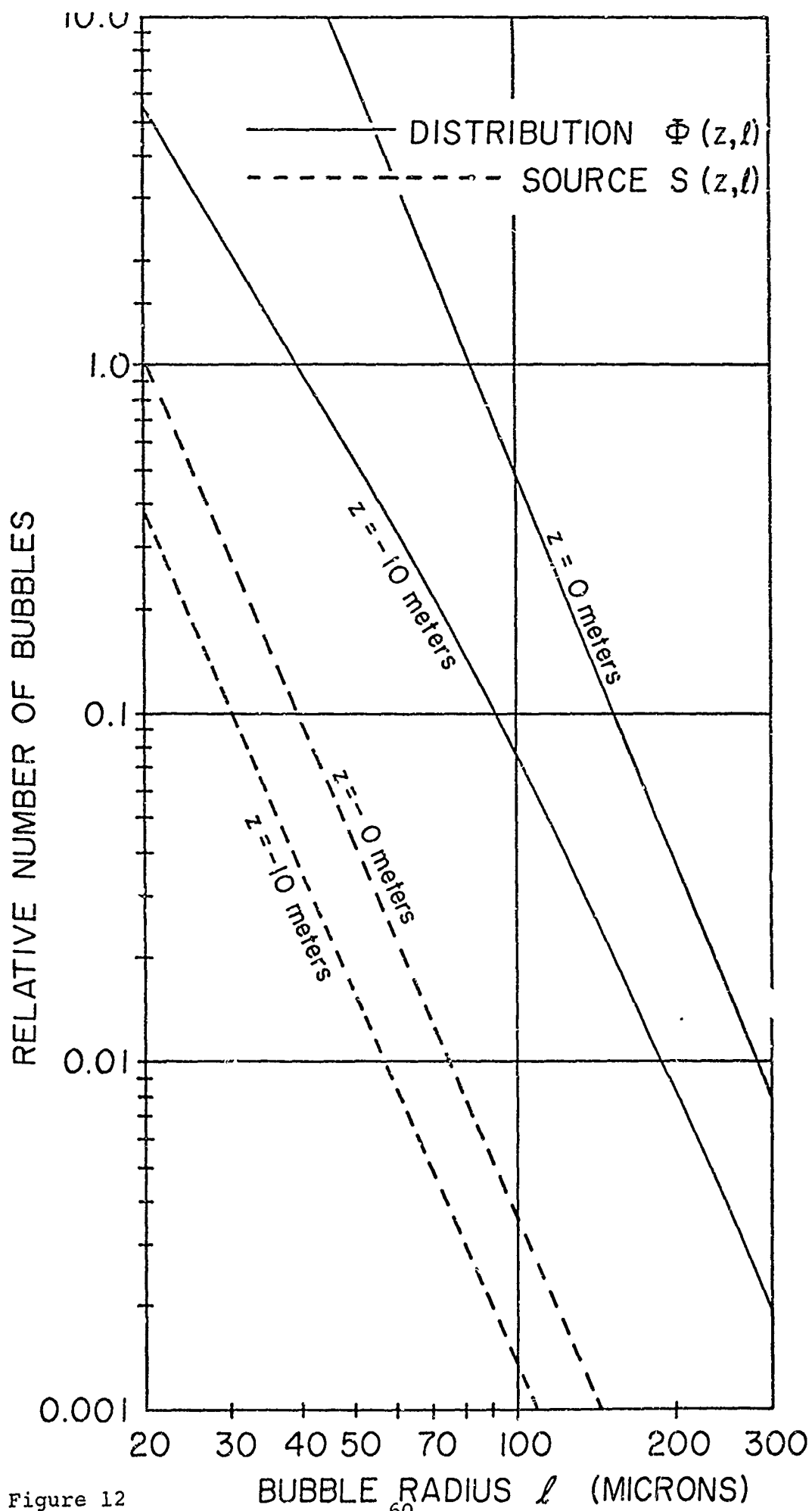


Figure 12